THE JOURNAL OF PHYSICAL CHEMISTRY B

Article

pubs.acs.org/JPCB

Radiation Stability of Cations in Ionic Liquids. 5. Task-Specific Ionic Liquids Consisting of Biocompatible Cations and the Puzzle of Radiation Hypersensitivity

Ilya A. Shkrob,*[,†] Timothy W. Marin,[†,‡] James F. Wishart,[§] and David C. Grills[§]

[†]Chemical Sciences and Engineering Division, Argonne National Laboratory, 9700 South Cass Avenue, Argonne, Illinois 60439, United States

[‡]Chemistry Department, Benedictine University, 5700 College Road, Lisle, Illinois 60532, United States

[§]Chemistry Department, Brookhaven National Laboratory, Upton, New York 11973-5000, United States

Supporting Information

ABSTRACT: In 1953, an accidental discovery by Melvin Calvin and co-workers provided the first example of a solid (the α-polymorph of choline chloride) showing hypersensitivity to ionizing radiation: under certain conditions, the radiolytic yield of decomposition approached 5×10^4 per 100 eV (which is 4 orders of magnitude greater than usual values), suggesting an uncommonly efficient radiation-induced chain reaction. Twenty years later, the still-accepted mechanism for this rare condition was suggested by Martyn Symons, but no validation for this mechanism has been supplied. Meanwhile, ionic liquids and deep eutectic mixtures that are based on choline, betainium, and other derivitized natural amino compounds are presently finding an increasing number of applications as diluents in nuclear separations, where the constituent ions are exposed to ionizing radiation that is emitted by decaying radionuclides. Thus, the systems that are compositionally similar to radiation hypersensitive solids are being considered for use in high radiation fields, where this property is particularly undesirable! In Part 5 of this series on organic cations, we revisit the phenomenon of radiation hypersensitivity and explore mechanistic aspects of radiation-induced reactions involving this class of task-specific, biocompatible, functionalized cations, both in ionic liquids and in reference crystalline compounds. We demonstrate that Symons' mechanism needs certain revisions and rethinking, and suggest its modification. Our reconsideration suggests that there cannot be conditions leading to hypersensitivity in ionic liquids.

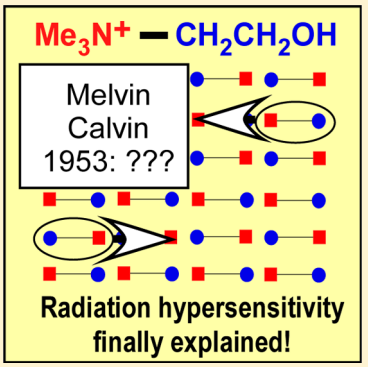

1. INTRODUCTION

Room-temperature ionic liquids (ILs) exhibit many desirable properties as diluents for liquid–liquid extractions of *f*-block elements in nuclear separations, including their low volatility, variable polarity, and high electric conductivity, and fire retardant properties.[1−4] During such separations, the extraction solvent is exposed to ionizing radiation that is generated by decaying radionuclide ions, and the long-term radiation stability of such IL diluents is a pressing concern in the development of robust IL-based extraction systems for advanced nuclear cycles.

In a series of publications from our two laboratories[5−8] we aimed to learn how structural variations in organic cations affect the radiation stability of ILs. In Part 5 of this series, we focus on functional modifications for the simplest of organic cations: tetraalkylammonium (Scheme 1) ions. As a rule, extracting agents and ionophores that contain ligands for metal ion extraction are introduced into diluents as *solutes*; however, the same ion-binding functionalities can be incorporated directly into the constituent ions. Such liquids are called task-specific ionic liquids (TSILs).[9−17] This synthetic strategy poses a question: which approach is preferable from the standpoint of radiation protection of the diluent and the extracting agent? We aim to begin answering this question.

Here we consider TSILs that are based on biologically compatible *N,N,N*-trialkylsubstituted amino alcohols and acids (such as choline and protonated betaine and carnitine shown Scheme 1) that have already found numerous applications.[12,15−23] Choline and betainium bistriflimides (Scheme 1) are poorly miscible with water at room temperature, but become fully miscible at a higher temperature, while remaining immiscible with nonpolar organic solvents over the entire temperature range.[19−23] Binnemans and co-workers[21,22] and Goff and co-workers[16,17] demonstrated how these unique properties can be used to sequester *d*- and *f*-elements, including lanthanide ions and uranyl ions. Shkrob et al.[23] demonstrated that such ILs can be used for group separations of trivalent lanthanide and actinide ions. Betainium ($Hbet^+$, Scheme 1) is a relatively strong acid (pK_a 1.84), and betainium bistriflimide (Hbet NTf_2) can dissolve metal oxides.[12,14−16] Deep eutectic solvents based on choline chloride have found many uses in polymer and synthetic organic chemistry[24] and electrochemistry.[25,26] In particular, choline chloride–urea eutectics

Received: May 20, 2014
Revised: August 14, 2014
Published: August 15, 2014

   dx.doi.org/10.1021/jp5049716 | J. Phys. Chem. B 2014, 118, 10477−10492

Scheme 1. Structural Formulas for Bistriflimide (NTf_2^-), Choline ($Chol^+$), and Zwitterionic and Protonated States of Betaine (bet) and Carnitine (car)

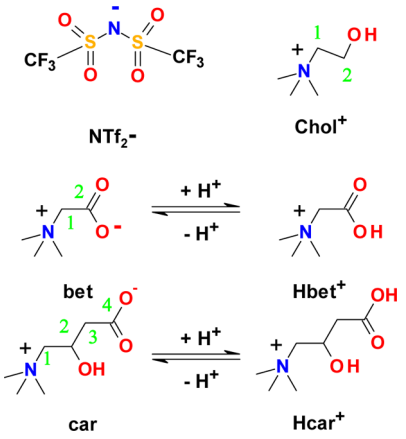

can also dissolve metal oxides, and the metal ions from these solutions can be reclaimed by electrodeposition.[27] Biocompatibility of choline-based ILs presents considerable interest for pharmaceutical applications.[28] We are confident that many other uses will be found for these new solvents; the question that we pose, however, is how does the functional derivatization of organic cations affect the TSILs that are based on these cations.

In the early 1950s, the great Melvin Calvin and his coworkers at the University of California at Berkeley developed their famous method for tracing biological metabolites using radioactive ^{14}C labeling. Most of these compounds were stable in their pure form, but one of them—the α-polymorph of crystalline choline chloride, α-Chol Cl (Scheme 1), decomposed rapidly after it crystallized from the solution,[29] with G values of cation loss approaching 5×10^4 species per 100 eV (vs the typical 1−5 species per 100 eV for organic compounds). This behavior was later named radiation hypersensitivity. Calvin challenged his colleagues to explain these surprising observations.[29−39] The task proved to be unexpectedly difficult. Twenty years later, using his new evidence from electron paramagnetic resonance (EPR) spectroscopy, Symons[40] suggested the currently accepted answer to Calvin's challenge.[36,37] The crucial insight is that radiolytic oxidation of choline can yield an unstable $Me_3N^+CH_2C^\bullet HOH$ radical that fragments along the C−N bond and releases vinyl alcohol, the enol form of acetaldehyde (see reaction Scheme 1S in the Supporting Information).

$$Me_3N^+CH_2C^\bullet HOH \rightarrow Me_3N^{+\bullet} + CH_2{=}CHOH \quad (1)$$

This enol isomerizes to acetaldehyde, while the radical cation of trimethylamine abstracts H from a nearby choline cation in the α-polymorph of the crystal[41−43]

$$Me_3N^{+\bullet} + Me_3N^+CH_2CH_2OH \rightarrow Me_3NH^+ + Me_3N^+CH_2C^\bullet HOH \quad (2)$$

initiating a self-propagating chain reaction through this crystal. In the absence of cross recombination, disproportionation, and chain terminating side reactions, reactions 1 and 2 would rationalize a high yield of cation decomposition per ionization event, so one way to account for radiation hypersensitivity is to assume that reactions 1 and 2 occur very rapidly on the time scale of these competing radical reactions. While this is a plausible and intellectually appealing rationale for the radiation hypersensitivity in α-Chol Cl, the validity of this proposition has never been demonstrated experimentally. If this proposition is correct, reactions 1 and 2 should pose an equally grave concern for the radiation stability of TSILs based on choline and similar functionalized cations, and these solvents would become unsuitable as diluents for nuclear separations. Interestingly, degradation of choline in some bacteria[44] also involves a radical H abstraction reaction similar to reaction 2 that involves a glycyl radical.[45,46]

Symons went further and suggested that the parent cation also undergoes radiolytic reduction (a dissociative electron attachment, DEA) that causes deamination, viz.

$$Me_3N^+CH_2CH_2OH + e^- \rightarrow Me_3N{+}^\bullet CH_2CH_2OH \quad (3)$$

The released β-hydroxyethyl radical abstracts H from the parent cation thereby yielding yet another seeding $Me_3N^+CH_2C^\bullet HOH$ radical cation that initiates reactions 1 and 2 within the same spur. This implies (though Symons did not posit this explicitly) that *both* oxidation and reduction of choline cations can start chain reactions propagating in different directions across the crystal.

The exceptional rarity of radiation hypersensitivity ensured little followup after the early 1970s; meanwhile the TSILs that are moving to center stage in present separation studies are alarmingly close structurally to ionic solids having this property. This consideration prompted us to revisit and further explore the radiation chemistry of such compounds.

To save space, many of the supporting tables, figures, details of synthetic and analytical protocols, and a list of abbreviations have been placed in the Supporting Information (SI).

2. PRELIMINARY CONSIDERATIONS

2.1. Symons' Rationale Challenged. Despite the conceptual simplicity of Symons' rationale for radiation hypersensitivity, other studies suggested a confluence of many factors at work (see Tables 1S and 2S in the Supporting Information).

In Chol Cl, radiation hypersensitivity was observed only in a narrow temperature range and only in the α-polymorph.[30−33,41,47] The hypersensitivity disappears somewhat below the α-to-β phase transition temperature,[39] when the reorientation (mainly, flip-flop)[48] motion of choline cations in the lattice becomes less arrested, as suggested by solid state NMR relaxometry.[48−50] The high-temperature β-polymorph is disordered, and there has been a long-standing conjecture that stereoselective effects play a significant role in its hypersensitivity.[32,39,41] While choline chloride and bromide exhibited high G values for cation decomposition, other salts (choline iodide, nitrate, acetate, and sulfate) yielded much lower decomposition yields (SI Table 1S). Even for Chol Cl, the cation decomposition was orders of magnitude less efficient in aqueous and alcohol solution (SI Table 2S), even at saturation, than in the crystal, suggesting that the postulated chain reaction did not propagate in solution. Doping of the crystal by electron scavengers and KI crystals inhibited radiolysis.[35] It was also much less efficient in large monocrystals relatively free of electron-trapping defects.[35] In low-temperature polycrystalline samples, the decomposition efficiency increased when the sample was exposed to infrared radiation, which suggests the

dx.doi.org/10.1021/jp5049716 | J. Phys. Chem. B 2014, 118, 10477−10492

involvement of trapped electrons.[35,38] The same is also suggested by radiothermoluminescence of these samples.[38]

Relatively high decomposition yields were also observed for $Me_3N^+CH_2CO_2H$ Cl and $Me_3N^+(CH_2)_3OH$ Cl crystals (SI Table 1S), whereas the radicals derived from the corresponding ions do not appear to have fragmentation reactions analogous to reaction 1. Furthermore, shortly after Symons suggested his chain reaction mechanism,[40] it was found that the presumably unstable $Me_3N^+CH_2C^{\bullet}HOH$ radical cation[36,37,51] (like many other similar species)[52,53] can be prepared and observed in aqueous solutions through the reaction of hydroxyl radicals with corresponding aminoethanols; there was no indication that these radicals decayed via very rapid reaction 1 except perhaps in strongly acidic solutions (pH < 1);[36] see section 2.3 for further discussion.

Symons assumed that oxidation of choline to $Me_3N^+CH_2C^{\bullet}HOH$ radical cation in Chol Cl was carried by radiolytically generated $Cl^{\bullet}$ atoms that abstract H more rapidly than they form $Cl_2^{-\bullet}$ radical anions (which were observed in EPR spectra).[54] This H abstraction reaction seems unlikely for $Br^{\bullet}$ atoms in Chol Br (as the H−Br bond is much weaker than the H−Cl bond) and it is positively impossible for $I^{\bullet}$ atoms (the latter may rationalize the much improved radiation stability of Chol I).[55,56] Judging from the much lower *G* values for choline decomposition, radiolytic generation of $Me_3N^+CH_2C^{\bullet}HOH$ (assuming Symons' mechanism) was suppressed in nitrate and sulfate crystals that are known to yield highly oxidizing radicals; furthermore, this oxidation definitely occurred in aqueous solutions, where these *G* values were also low. A possible rationale would be rapid deprotonation of $Me_3N^{+\bullet}$ cation to give the $Me_2N^{\bullet}CH_2$ radical, but even this secondary radical can abstract H from choline cation, sustaining the chain reaction.

All of these observations taken together cast doubt that Symons' rationale for radiation hypersensitivity is entirely correct. At face value it appears that reaction 1 can occur only in certain solid matrices under very special conditions, for uncertain reasons.

2.2. A Sketch of Radiation Chemistry. Before progressing further, we briefly examine the general pattern of radiation damage reactions in organic ionic compounds.[57] SI Tables 3S to 8S summarize computational data on energetics and magnetic parameters of the species involved (see section 3 for methods).

Interaction of ionizing radiation with matter generates highly excited states that dissociate through fragmentation or undergo autoionization. The released electrons have significant excess energy before they thermalize and localize in the matrix, and dissociative electron attachment (DEA) reactions like reaction 3 are possible. No DEA-induced deamination has been observed in radiolysis of tetraalkylammonium cation-based ILs,[58] whereas the loss of the aliphatic arms that is concerted with the H transfer does occur in the electronically excited cations.[57] The analogous reaction for choline would be

$$\{Me_3N^+CH_2CH_2OH\}^{**} \rightarrow Me_3NH^+ + CH_2{=}CHOH \text{ or } MeCHO \quad (4)$$

This reaction yields the same stable products as reactions 1 and 2. Also possible is homolytic C−N bond scission reaction 5

$$\{Me_3N^+CH_2CH_2OH\}^{**} \rightarrow Me_3N^{\bullet+} + {}^{\bullet}CH_2CH_2OH \quad (5)$$

that yields the same radical products as reactions 1 and 3. Due to the possible occurrence of such reactions, observation of the corresponding species does not necessarily implicate reactions 1 to 3.

"Ionization" of the organic cation (C^+) generally causes rapid deprotonation and the formation of an H-loss radical.

$$\{C^+\}^*A^- \rightarrow e^{-\bullet} + C(-H)^{+\bullet} + H^{\delta+}A^{\delta-} \quad (6)$$

The same $C(-H)^{+\bullet}$ species can be formed when oxidized anion (A^-) abstracts H from the same cation

$$C^+\{A^-\}\ ^* \rightarrow e^{-\bullet} + C^+ + A^{\bullet} \quad (7)$$

$$C^+ + A^{\bullet} \rightarrow C(-H)^{+\bullet} + H^{\delta+}A^{\delta-} \quad (8)$$

For carboxylated cations (such as betainium and carnitinium), oxidation can also release CO_2 via a Kolbe reaction, e.g.,

$$\{Me_3N^+CH_2CO_2^-\}^*A^- \rightarrow e^{-\bullet} + Me_3N^{+\bullet}CH_2A^- + CO_2 \quad (9a)$$

$$\{Me_3N^+CH_2CO_2H\}^*A^- \rightarrow e^{-\bullet} + Me_3N^{+\bullet}CH_2 + CO_2 + H^{\delta+}A^{\delta-} \quad (9b)$$

The ${}^{\bullet}CH_2CO_2H$ radical would be expected to originate through a fragmentation reaction analogous to reaction 5 or from a DEA reaction analogous to reaction 3 that involves the electrons released in reactions 6, 7, and 9b

$$Me_3N^+CH_2CO_2H + e^{-\bullet} \rightarrow Me_3N + {}^{\bullet}CH_2CO_2H \quad (10)$$

The occurrence of reaction 10 is not a given, as carboxylic acids (like many other acids in radiolysis) can also react through the release of H atoms, viz.

$$Me_3N^+CH_2CO_2H + e^{-\bullet} \rightarrow Me_3N^+CH_2CO_2^- + H^{\bullet} \quad (11)$$

The mobile $H^{\bullet}$ atom abstracts H from the parent cation yielding the same $C(-H)^{+\bullet}$ cations that are generated in the "ionization" of these parent cations (reactions 7 and 8), leaving no distinct signature of the involvement. In the gas phase, reaction 10 is ∼2.3 eV more exergonic than reaction 11, and it seems unlikely that the stabilization in the matrix can offset this energy difference. Formation of ${}^{\bullet}CH_2CO_2H$ in radiolysis of sarcosine chloride and glycine chloride has been observed[54,59−63] and it is known to occur in their aqueous solutions too.[64−66] Analogous deamination reactions occur in radiolysis of other α-amino acids, but not β-amino acids.[61]

It is likely that deamination can also occur in betainium compounds. In irradiation of glycine chloride at 4 K, it is possible to observe unstable $H_3N^+CH_2{}^{\bullet}CO_2H^-$ radical or perhaps the $H_3N^+CH_2{}^{\bullet}CO_2^{2-} + H^+$[67] intermediate of reaction 11 before the deamination sets in; the latter reaction is complete at 110 K.[54] The same two species were observed in radiolysis of glycine[62] where they coexist with the products of decarboxylation (reactions 9a and 9b) and deprotonation (reaction 6).[53,61,62,68] The metastable intermediate of reaction 11 can be sometimes stabilized by the matrix, decaying only at 150−180 K.

The situation is more complex for choline-based ILs, where DEA reaction 3 can be expected to compete with electron solvation in these ILs. In liquid[69] and vitreous aliphatic alcohols[70−74] and polyols,[73,75−79] electrons self-trap in solvent voids via the formation of the so-called "solvated/trapped electron" in which several hydroxyl dipoles acting in concert

dx.doi.org/10.1021/jp5049716 | J. Phys. Chem. B 2014, 118, 10477−10492

stabilize the *s*-electron that fills the void. Similar excess electron species are also formed in void-like defects in certain polyol crystals[80] and ice.[81] This possibility has already been discussed by Lemmon and co-workers[35,38] who obtained indirect evidence for the involvement of electron trapping in radiolysis.

More recently, trapped and solvated electrons have been observed in ILs that consist of aliphatic cations (such as cyclic and acyclic tetraalkylammonium cations).[82−87] Electrons in such media can be stabilized via electrostatic interactions with the positive charges in heteroatoms of the cations (like F-centers in alkali halide crystals) or through interaction with the induced C−H dipoles in their aliphatic arms (as occurs in electrons trapped in alkanes).[88,89] It is well-known that both ground and photoexcited[90] trapped/solvated electrons ($e_{solv}^{-\bullet}$) in solid and liquid alcohols (ROH) eventually undergo a proton transfer reaction yielding the H$^\bullet$ atom and the RO$^-$ anion. This reaction is known to occur both in alcohols (see Table 7.6 in ref 91) and in polyol single crystals.[92−94]

An analogous reaction involving choline cation would be

$$Me_3N^+CH_2CH_2OH + e_{solv}^{-\bullet} \rightarrow Me_3N^+CH_2CH_2O^- + H^\bullet$$

Unlike betaine (that has stable zwitterion form), the zwitterion of choline is unstable (in the gas phase this reaction is endergonic by 1.9 eV; see SI Table 5S)

$$Me_3N^+CH_2CH_2O^- \rightarrow Me_3N + CH_2{=}CHOH$$

and the overall DEA reaction would be

$$Me_3N^+CH_2CH_2OH + e_{solv}^{-\bullet} \rightarrow Me_3N + CH_2{=}CHOH + H^\bullet \quad (12)$$

The released H atom can add to the enol double bond, yielding $^\bullet CH_2CH_2OH$ radical (in this case, the overall reaction is indeed reaction 3), but it can also abstract H from the parent cation, yielding the chain-sustaining $Me_3N^+CH_2{}^\bullet CHOH$ radical cation (reaction 1). Reaction 12 can leave no discernible EPR signature, as the H$^\bullet$ atom is converted to the same radicals that are generated via oxidation of the parent cation. In this way, radiolytic reduction can increase the decomposition of cations via reactions 1 and 2 in a manner envisioned by Symons, however, without the concomitant reaction 3 occurring.

Turning to oxidation, for betaine/betainium we suggested the formation of the internal radical and also several terminal ($^\bullet CH_2R$) radicals (see above). The latter radicals are reactive, and they would readily abstract H from the parent cation, generating the internal radical

$$Me_3N^+CH_2CO_2H + {}^\bullet CH_2R \rightarrow Me_3N^{+\bullet}CHCO_2H + CH_3R \quad (13)$$

Analogous secondary reactions can be expected for choline and carnitinium. Such reactions are well-known from the radiation chemistry of natural α-amino acids.[59,61,68] One can expect that only this internal radical can persist when other radicals become mobile and undergo reaction 13 (in analogy to the corresponding radical for glycine),[61] as this radical cannot readily disproportionate or recombine with other species than H$^\bullet$ and $^\bullet CH_2CO_2H$.

2.3. Identity of the "Persistent Radical" in α-Chol Cl Challenged. For choline, the one-electron oxidation can potentially involve all of the C−H bonds in this cation. In aqueous solution, the HO$^\bullet$ radical selectively oxidizes (alkyl- or H- substituted) $R_1R_2R_3N^+CH_2CH_2OH$ cations to $R_1R_2R_3N^+CH_2{}^\bullet CHOH$ radical cation.[36,51−53,95] This carbon-2 centered radical species (Scheme 1) is stable in solution; only for $Et_3N^+CH_2CH_2OH$ were some secondary $Et_3N^{+\bullet}$ radicals observed in the reaction mixture. Foster and West[36] suggested that reaction 1 in choline containing crystals proceeds via the formation of Me_3N and a $CH_2CHOH^{+\bullet}$ intermediate that forms only in such crystals, but this seems very unlikely energetically.

The preferential formation of a H-loss radical at the carbon-2 atom[36] follows the general pattern for aminated compounds;[52,53] it is attributed to the kinetic control of H atom abstraction. In the gas phase (SI Table 3S), we estimate that the X−H bonds have energies of 4.19, 4.73, 4.92, and 4.93 eV for C_2−H, C_1−H, C_N−H, and O−H bonds, respectively, so H−C_2 abstraction is greatly preferred energetically. The C_1−N bond dissociative H abstraction from carbon-2 corresponds to 4.99 eV for the enol form and 4.45 eV for the keto form elimination of the acetaldehyde (SI Table 3S). In the lowest energy conformer of gas-phase $Me_3N^+CH_2{}^\bullet CHOH$ radical, the O−C_2−C_1−N dihedral angle is 83.4°, which is very close to the analogous angle for the parent cation in α-Chol Cl.[42,43] This dihedral angle is ∼0° in the radiation-stable β-polymorph of Chol Cl that is observed at temperatures above 78 °C.[41]

Our DFT calculations (Figures 1 and 2a) indicate a rotation barrier of 0.32 eV for O−C_2−C_1−N rotation where the crests

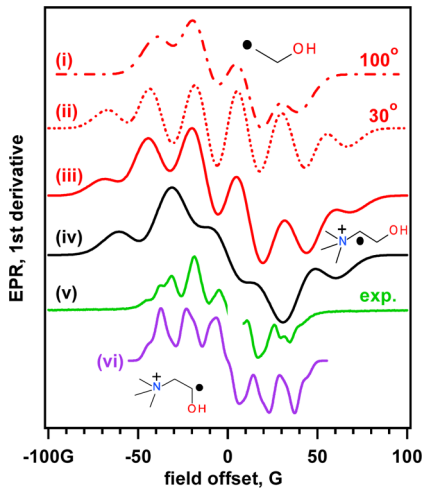

Figure 1. (a) Simulated first-derivative EPR spectra using hfcc's tensors calculated for gas phase (i−iii) $^\bullet CH_2CH_2OH$, (iv) $Me_3N^{+\bullet}CHCH_2OH$, and (vi) $Me_3N^+CH_2{}^\bullet CHOH$ radicals (assuming spherical *g*-tensors). The latter radical is in the lowest-energy conformation with the O−C_2−C_1−N angle of 84°. Traces (i) and (ii) correspond to H_α−C−C−O dihedral angle of 100° and 30°, respectively. Traces (iii) and (iv) correspond to an ensemble of radicals with random dihedral angles. Trace (v) shows the experimentally observed spectrum.

correspond to the in-plane conformations, at which dissociation to $Me_3N^{+\bullet}$ + MeCHO, but not to $Me_3N^{+\bullet}$ + $CH_2{=}CHOH$, becomes energetically feasible (Figure 2a). Additional energy is available through polarization effects, as the $Me_3N^{+\bullet}$ cation is smaller than the $Me_3N^+CH_2{}^\bullet CHOH$ cation. It seems unlikely, however, that despite this additional driving force, reaction 1 can occur as written in many polar media; it may involve isomerization of the enol to keto form in concert with C_1−N

dx.doi.org/10.1021/jp5049716 | J. Phys. Chem. B 2014, 118, 10477−10492

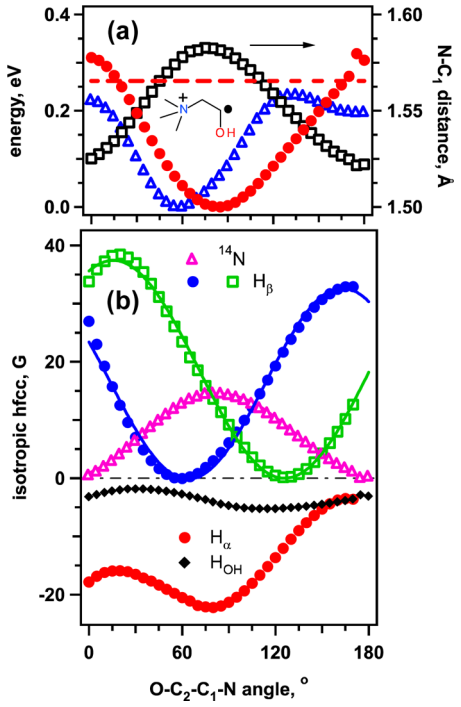

Figure 2. Energetics and isotropic hyperfine coupling constants computed for gas phase $Me_3N^+CH_2^\bullet CHOH$ radical cation (B3LYP/6-31+G(d,p) method) as a function of the O−C_2−C_1−N dihedral angle (all other degrees of freedom optimized). In panel (a), filled circles and open triangles indicate conformation energy for the radical cation and parent cation, respectively (to the left), and open squares indicate the N−C_1 bond length (to the right). The dashed lines indicate energy of dissociation to $Me_3N^{+\bullet}$ radical cation and acetaldehyde. Panel (b) shows the angular dependencies for ^{14}N, $^1H_{OH}$, and $^1H_{\alpha,\beta}$ nuclei in this radical. The solid lines are sine dependencies. The computed hfcc's at the bottom of the potential well correspond to the ones obtained in solution for this radical cation.

bond dissociation, as otherwise the reaction becomes too endergonic.

$$\{Me_3N^+CH_2^\bullet CHOH\}A^- \rightarrow \{Me_3N^{+\bullet}\}A^- + MeCHO \quad (14)$$

This may explain the importance of low pH, which is required to observe this reaction in aqueous solutions, suggesting that it involves proton catalysis.[115]

Radiolysis of α-Chol Cl yields one principal progenitor radical (known as "persistent radical") that is observed in EPR spectra obtained over a wide temperature range. In SI Figure 1S we replot the spectral data for four H/D substituted isotopomers of choline. This persistent radical was attributed to the β-hydroxyethyl radical[29] with anomalously small hyperfine coupling constants (hfcc's) for $^1H_\beta$ protons:[40] instead of the typical values of 27−32 G reported (SI Table 4S) and/or estimated (SI Table 5S) in this radical, one would need hfcc's of just 14 G, which is possible only if the H_α−C−C−O dihedral angle is close to 90° (SI Figure 2S), whereas the preferred orientation is nearly in-plane (0−30°). In SI Figure 3S, we show simulated EPR spectra for this radical assuming a Boltzmann factor weighting in an ensemble of rotationally arrested conformers in the matrix, and in Figure 1 we compare the EPR spectra for "free" rotation, a fixed (lowest-energy) 30° conformer and the postulated 90−100° conformer (traces ii and i, respectively) with the experimental EPR spectrum of the persistent radical (trace (v). It is seen that neither of these EPR spectra resembles the experimental EPR spectrum. Our conclusion is consistent with an EPR study on irradiated $H_2NCO_2CH_2CH_2N^+Me_3$ Cl monocrystals[96] that failed to observe $-CH_2^\bullet CH_2$ terminated radicals in this closely related system.

Two other possible candidates for this radical are $Me_3N^+CH_2^\bullet CHOH$ and $Me_3N^{+\bullet}CHCH_2OH$ radical cations. For the latter, the preferred conformer has an O−C_1−C_2−N angle of 30° (SI Figure 4S), which yields a triplet (SI Figure 5S). As the rotation barrier is only 0.2 eV, it is possible that other conformers could be present in the matrix, and in EPR simulations shown in SI Figure 5S, we "freed" the rotation as a function of temperature, as more energy becomes available. It is seen from comparisons made in Figure 1 that this simulated EPR spectrum is also unlike the experimental one.

By exclusion, this leaves the $Me_3N^+CH_2^\bullet CHOH$ radical cation. Figure 2a indicates that the preferred conformer has ~90° dihedral angle, at which the calculated hfcc's are very close to those reported in aqueous solutions (Figure 2b and SI Tables 4S and 5S). As the potential well is deep for this radical (Figure 2a), this conformer is a good representative for the entire ensemble of conformers (SI Figure 6S). The hfcc tensors for magnetic nuclei in this conformer are given in SI Table 6S. Simulated EPR spectra closely reproduce the experimental ones (compare the 300 K trace in SI Figure 6S with SI Figure 1S and the spectrum for the 90° conformer vs the experimental spectrum in Figure 1). In SI Figure 7S, we simulated EPR spectra for this conformer using the same four isotope configurations shown in SI Figure 1S. The trends observed upon H/D substitution are identical in both sets of the EPR spectra.

We conclude that the "persistent radical" observed in α-Chol Cl is the $Me_3N^+CH_2^\bullet CHOH$ radical in its lowest energy conformation. This radical is stable in the crystalline matrix, which calls into question the premise of the presently accepted scenario of radiation hypersensitivity.

3. EXPERIMENTAL AND COMPUTATIONAL METHODS

Synthetic procedures and spectroscopic data for bistriflimides of the cations shown in Scheme 1 are given in section 1S of ref 23. Differential scanning calorimetry data (SI Figure 8S) were obtained using a TA Instruments Q100 DSC with LNCS cooling system and a scan rate of 5 °C/min. A previous report placed the melting point of Chol NTf_2 at 27 °C,[97] however, scans on two separate samples prepared in our laboratory from the metathesis of Chol Cl and Li NTf_2 following the procedures in that paper showed a melting point of 38 °C and sharp solid−solid phase transitions at 1 and 26 °C (all temperatures onset). It was found that Chol NTf_2 could persist at room temperature as a supercooled liquid for some time if not mechanically disturbed. The glass transition temperature for vitreous flash-frozen Chol NTf_2 is 190 K.

The experimental and computational approaches used in the present study were similar to these used in Parts 1 and 2 of this series.[5,6] For EPR spectroscopy, the IL samples were heated to 60 °C and then frozen by rapid immersion in liquid nitrogen; the chlorides were irradiated as powdered polycrystalline solids. These samples were irradiated to 3 kGy at 77 K (or 300 K, where specified). The radicals were observed using a 9.44 GHz Bruker ESP300E spectrometer, with the sample placed in a flow helium cryostat (Oxford Instruments CF935). The magnetic field and the hfcc's are given in units of Gauss (1 G = 10^{-4} T).

dx.doi.org/10.1021/jp5049716 | J. Phys. Chem. B 2014, 118, 10477−10492

If not stated otherwise, the first-derivative EPR spectra were obtained using 0.02 mW of microwave power and 2 G modulation at 100 kHz at 50 K. The radiation-induced EPR signal from the E'_γ center and H• atoms in the Suprasil sample tubes is shadowed white in some of the EPR spectra.

The calculations of hyperfine coupling (hfc) tensors ***A*** and radical structures were carried out using a density functional theory (DFT) method with the B3LYP functional[98,99] and 6-31+G(d,p) basis set from Gaussian 03;[100] a_{iso} denotes the isotropic hfcc corresponding to the hfc tensor and ***B*** denotes the anisotropic part of this tensor. Powder EPR spectra were simulated using first-order perturbation theory assuming isotropic ***g***-tensors and anisotropic hfcc tensors for ^{1}H and ^{14}N nuclei. In SI Table 4S, we list the reported isotropic hfcc's for the reference radicals, and in SI Table 5S give the hfcc's obtained in our density functional theory (DFT) calculations for gas-phase radicals; the overall agreement is very good. The energetics of these species and their selected reactions are summarized in SI Tables 3S, 7S, and 8S.

Pulse radiolysis transient absorption (TA) studies were performed at the BNL Laser-Electron Accelerator Facility (LEAF) as previously described.[5,101,102] UV−vis-NIR (ultraviolet−visible−near-infrared) TA measurements were performed on argon-purged samples of Chol NTf_2 in septum-sealed, Suprasil self-masking semimicro 1 cm spectrophotometer cuvettes. TA signals were recorded using 8 nm optical bandpass filters, an FND-100Q silicon photodiode, a CLC-100 amplifier, a Teledyne LeCroy HRO 66Zi 12-bit oscilloscope, and locally written LabVIEW (National Instruments, Inc.) and Igor Pro (Wavemetrics, Inc.) code for acquisition and analysis, respectively. Dosimetry was calculated on the basis of the absorbance of the thiocyanate dimer radical anion ($(SCN)_2^{\bullet-}$, $\varepsilon_{480\ nm}$ = 7950 M^{-1} cm^{-1}) produced in N_2O-saturated aqueous 10 mM KSCN solution (G = 6.13 × 10^7 mol J^{-1}).

Time-resolved infrared (TRIR) transient absorption pulse radiolysis was carried out on a new beamline at LEAF dedicated for this experiment. The general proof-of-concept of the detection system, which uses quantum cascade lasers as tunable sources for the IR analyzing light, was described previously.[103] The new instrumentation will be the subject of a subsequent publication; however, a brief but detailed description is given in the Supporting Information of a recent communication.[104] The Chol NTf_2 sample was contained in a home-built, airtight IR solution flow cell equipped with 0.35-mm-thick CaF_2 windows separated by 1.1 mm Teflon spacers. A 1.0 mL Hamilton Gastight syringe was charged in a glovebox with argon-purged Chol NTf_2 warmed to 60 °C and connected to the flow cell. The TRIR measurements were complicated by the fact that Chol NTf_2 is a solid at room temperature (SI Figure 8S). For this reason, the entire flow system was thermostated to 50 °C. Two detectors (KMPV9-0.5-J2, Kolmar Technologies, Inc.) were used for sample and reference channels in order to minimize the effect of laser fluctuations. The signals were acquired and processed with the same HRO 66Zi oscilloscope and software as the UV−vis−NIR TA system. Static infrared spectra were recorded using a Thermo Scientific Nexus 670 FTIR spectrometer. The extinction coefficient of the acetaldehyde C═O stretching band was determined to be 189 M^{-1} cm^{-1} at the peak of 1721 cm^{-1}, using a 0.179 M solution in ethanol in with a 0.275 mm path length cell. Ethanol was used as a surrogate alcohol solvent in place of Chol NTf_2 because the boiling point of acetaldehyde (21 °C) is well below the 38 °C melting point of Chol NTf_2, making it difficult to accurately prepare a solution of known concentration. We assume for the sake of argument that the extinction coefficient in Chol NTf_2 is approximately the same as in ethanol.

4. RESULTS

4.1. Betainium Compounds. For betainium cation, there are two variants of H-loss radical, $Me_2(^\bullet CH_2)N^+CH_2CO_2H$ and $Me_3N^{+\bullet}CHCO_2H$. The latter species is analogous to the persistent glycyl ($H_3N^{+\bullet}CHCO_2H$) radical in irradiated solid glycine (section 2.2). The corresponding EPR spectra are simulated in SI Figure 9S. It is seen from SI Tables 4S and 5S that for C_1 and C_{Me} (Scheme 1) centered radical cations the hfcc's on the ^{14}N and methyl protons are negligible, and the EPR spectra originate through coupling on the $^1H_\alpha$ nuclei (we adopt the common EPR notation in which α relates to the locus of the unpaired electron density). Thus, the $Me_3N^{+\bullet}CHCO_2H$ radical cation appears as a doublet, whereas $^\bullet CH_2CO_2H$, $^\bullet CH_2CO_2^-$, $Me_2(^\bullet CH_2)N^+CH_2CO_2H$, and $Me_3N^{+\bullet}CH_2$ radicals appear as triplets (see simulations in SI Figure 9S). In SI Figure 10S, photoactivated anatase nanoparticles (355 nm laser excitation) were used to oxidize betaine and betainium (chloride) in frozen aqueous solutions. For other amino acids, this photoreaction has always been the photo-Kolbe reaction (which is analogous to reactions 9a and 9b)[105,106] and we expect that the resulting triplet in the EPR spectrum is from the $Me_3N^{+\bullet}CH_2$ radical cation, which is also consistent with the simulations shown in SI Figure 9S.

SI Figure 11S demonstrates first-derivative EPR spectra obtained in low-temperature radiolysis of crystalline betaine and betainium chloride. It is seen that several species contribute to these composite EPR spectra that can be considered as overlapping signals from the doublet of $Me_3N^{+\bullet}CHCO_2(H)$ radical cation and triplet(s) of $^\bullet CH_2R$ radicals. As the temperature increases over 120 K (SI Figure 12S), the triplet progenitors disappear from the EPR spectra, but the betainyl doublet (indicated with the open circles in SI Figures 12S and 13S) persists to 300 K. This is consistent with thermally activated H abstraction by the terminal radicals (analogous to reaction 13), which is also known to occur for glycine. In addition to this doublet, there is a set of narrow resonance lines that belongs to the $Me_3N^{+\bullet}$ radical cation and (on a much wider field scan) the multiplet of the $Cl_2^{-\bullet}$ radical anion (not shown). The $Me_3N^{+\bullet}$ and betainyl radical cations are also observed in the irradiated betaine that is annealed at 300 K (SI Figure 13S). Since the $Me_3N^{+\bullet}CHCO_2(H)$ radical cannot undergo a fragmentation reaction similar to reaction 1, there should be a reaction pathway for generation of the $Me_3N^{+\bullet}$ radical cation other than reaction 1. The observed low yield of this species may be caused by its reactivity toward the parent cation in reaction 15 that is analogous to reaction 2 for choline

$$Me_3N^{+\bullet} + Me_3N^+CH_2CO_2H \rightarrow Me_3NH^+ + Me_3N^+C^\bullet HCO_2H \quad (15)$$

This yield becomes still lower when the crystals are irradiated at 300 K, suggesting that most of the generated $Me_3N^{+\bullet}$ radical cations are consumed in reaction 15 under such conditions. The same thermal cycle (that is, electron irradiation at 77 K followed by 300 K anneal) yields these radical cations for crystalline Chol Cl and Hcar Cl (SI Figure 14S) and for these two compounds the $Me_3N^{+\bullet}$ species readily survive in room-temperature radiolysis (Figure 3), where they make the predominant contribution to the observed EPR spectra.

dx.doi.org/10.1021/jp5049716 | J. Phys. Chem. B 2014, 118, 10477−10492

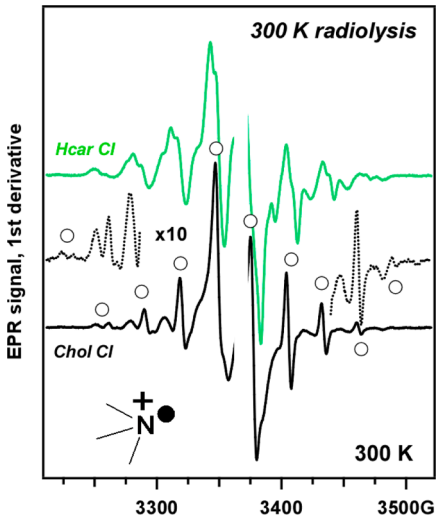

Figure 3. First-derivative EPR spectra of Chol Cl and Hcar Cl irradiated and obtained at 300 K. Open circles indicate well-resolved resonance lines of the $Me_3N^{+\bullet}$ radical cation generated in radiolysis of Chol Cl. Line broadening is stronger for Hcar Cl due to more hindered rotation of the methyl groups in this radical cation.

These observations are difficult to accommodate in Symons' mechanism, as very rapid and efficient reaction 2 needs to occur for the chain reaction to propagate.

Turning to the ILs, Figure 4 shows the EPR spectrum of irradiated frozen Hbet NTf_2. In the wings, there are multiple

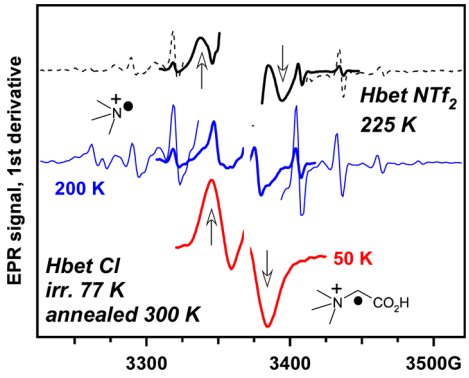

Figure 4. First-derivative EPR spectra in Hbet NTf_2 irradiated at 77 K (observed at 225 K) and Hbet Cl irradiated at 77 K, annealed at 300 K, and observed at 50 and 200 K, as indicated in the plot. The arrows indicate the doublet of $Me_3N^{+\bullet}CHCO_2H$ radical, the set of narrow resonance lines in the two upper traces (magnified) are from the $Me_3N^{+\bullet}$ radical cation. At 50 K, slow rotation of methyl groups causes line broadening, and only the betainyl radical is observed. The resonance line of the $^{\bullet}SO_2NHTf$ radical is excluded from the upper trace.

resonance lines of the $^{\bullet}CF_3$ and $^{\bullet}CF_2SO_2NTf^-$ radicals that are also observed in all other irradiated bistriflimide compounds and originate through the fragmentation of the bistriflimide anion via reactions[55,57,58]

$$\{NTf_2^-\}^{**} \rightarrow {}^{\bullet}CF_3 + {}^{\bullet}SO_2NTf^- \quad (16)$$

$$NTf_2^- + e^{-\bullet} \rightarrow F^- + {}^{\bullet}CF_2SO_2NTf^- \quad (17)$$

Due to the large hfcc's on ^{19}F nuclei, the resonance lines of these radicals do not interfere with the resonance lines from organic radicals derived from the cation. It is seen from Figures 4 and 15S that the latter EPR spectrum is most consistent with the $Me_3N^{+\bullet}CH_2$ radical cation (SI Figure 10S). The occurrence of oxidative decarboxylation in the parent cation is also suggested by generation of CO_2 in the sample, as gas bubbles form when the irradiated sample thaws. Warming of the irradiated sample to 175 K does not change the appearance of this triplet spectrum; however, as the signal decays, one begins to observe masked resonance lines from the $Me_3N^{+\bullet}$ radical cation that become fully resolved at 150 K (SI Figures 15S and 16S), but these can be observed even at a lower temperature, when the lines become considerably broadened due to hindered rotation in the methyl groups. This suggests that the $Me_3N^{+\bullet}$ radical cation is generated promptly (as opposed to a thermally activated secondary reaction like reaction 1), and postulated excited state reaction 5 can be the source of this species in low-temperature radiolysis. As can be seen from SI Figures 15S and 16S, the yield of this species is very low relative to the progenitor of the triplet, so the $^{\bullet}CH_2CO_2H$ radical that is a byproduct of reaction 5 cannot account for the triplet. We remind, however, that this radical can also be generated in reaction 10.

The complexity of the EPR spectra obtained in low-temperature irradiated betaine and Hbet Cl suggests that at least two kinds of $^{\bullet}CH_2R$ radicals contribute to the overall EPR spectrum in these solids. In the case of irradiated Hbet NTf_2, it is, however, less obvious that DEA reaction 10 can take place since energetic electrons involved in this DEA reaction can also be consumed in an alternate DEA reaction 17 that competes with it. The consistency of the spectrum envelope during the programmed warming of the irradiated sample suggests the presence of a single radical progenitor that can only be the $Me_3N^{+\bullet}CH_2$ radical cation.

We, therefore, conclude that the "holes" (electron deficiencies) in Hbet NTf_2 overwhelmingly react with the *carboxyl groups* of the parent cation. There seems to be little or no generation of the $Me_3N^{+\bullet}CHCO_2H$ radical cation or $^{\bullet}NTf_2$ radical[55,58,107] (which is generated via reaction 7). In the gas phase (SI Table 7S), $Me_3N^{+\bullet}CH_2 + CO_2$ has 0.28 eV lower energy than the $Me_3N^{+\bullet}CHCO_2H$ radical cation, i.e., reaction 9b is more exergonic than reaction 6. It should be even more exergonic in the ionic matrix, because the smaller $Me_3N^{+\bullet}CH_2$ cation interacts with anions in the matrix more strongly than the larger $Me_3N^{+\bullet}CHCO_2H$ cation. As the sample temperature increases to 200 K, the triplet signal decays, and the EPR spectrum shown in SI Figure 17S consists of the overlapping resonance lines of the $Me_3N^{+\bullet}$ radical cation and the familiar doublet of the $Me_3N^{+\bullet}CHCO_2H$ radical cation (generated via reaction 13 involving the $Me_3N^{+\bullet}CH_2$ radical). There is also a characteristic resonance line that we previously attributed to $^{\bullet}SO_2NHTf$ (which is a protonated form of the radical anion fragment generated in reaction 17).[108] The identity of the cation derived radicals transpires from a comparison (Figure 5) to the same species observed in irradiated Hbet Cl.

Our conclusion is that the radiation chemistry of betainium cations in Hbet NTf_2 is quite simple: these cations are oxidized to $Me_3N^{+\bullet}CH_2$ radical cations that subsequently abstract H from the progenitor cations and yield persistent $Me_3N^{+\bullet}CHCO_2H$ radical cations. A reaction of the excited state cations yields $Me_3N^{+\bullet}$ and (presumably) $^{\bullet}CH_2CO_2H$ radicals; the yield of these two species is quite low. There seems to be no or very little deamination (e.g., due to the competitive defluorination of the anion).

dx.doi.org/10.1021/jp5049716 | J. Phys. Chem. B 2014, 118, 10477−10492

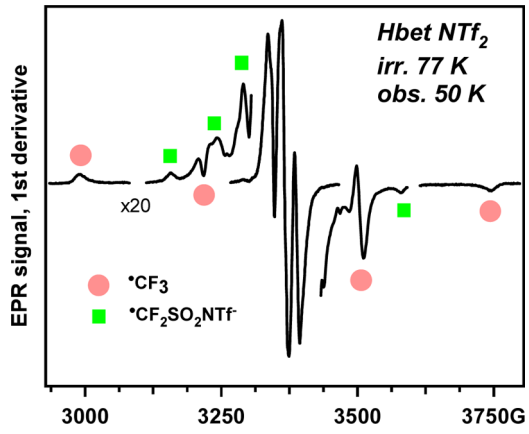

Figure 5. First-derivative EPR spectrum of Hbet NTf_2 irradiated at 77 K and observed at 50 K. The filled circles and squares indicate bistriflimide-derived radicals indicated in the plot. The resonance lines of the $H^•$ radicals are blotted out. Note 20× magnification for the wings.

4.2. Choline Compounds. *4.2.1. Matrix Isolation EPR Spectroscopy.* Irradiation of Chol NTf_2 is also surprisingly "clean": as seen from Figure 6a, it yields the same $•CF_3$ and $•CF_2SONTf^-$ radicals that are observed in other bistriflimide compounds, and in addition to these two anion-derived species there is an organic radical(s) whose EPR spectrum is very similar to that observed in irradiated α-Chol Cl (Figure 6b) that in section 2.3 was identified as the $Me_3N^+CH_2•CHOH$ radical cation generated via reactions 6 or 8. In irradiated α-Chol Cl,

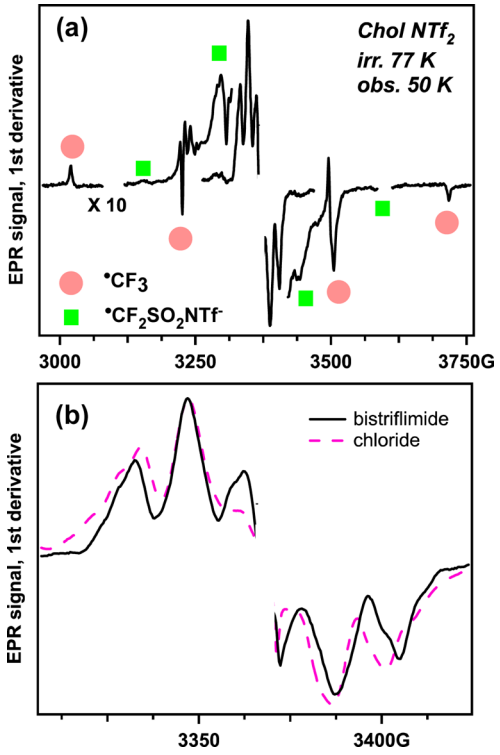

Figure 6. (a) First-derivative EPR spectra of frozen ionic liquid Chol NTf_2 irradiated at 77 K and observed at 50 K. Filled circles and squares indicate bistriflimide-derived radicals indicated in the plot. (b) Central section of the EPR spectrum shown in panel (a) (solid line) compared to the EPR spectrum obtained in irradiated α-Chol Cl under the same conditions.

the appearance of this EPR spectrum does not change considerably at 50 and 225 K (suggesting that the rotation effects are minor; see SI Figure 18S) and this shape is practically unchanged even after room-temperature annealing (SI Figure 18S). As the Chol NTf_2 matrix softens at the glass transition temperature of 190 K, we cannot establish the latter for the IL matrix, as the radical decays, but as SI Figure 19S demonstrates, there is little evolution of the spectral envelope between 50 and 200 K, and the behavior is identical to the same radical species in crystalline Chol Cl. It is seen that the identity of the persistent radical is the same in both solids, that is $Me_3N^+CH_2•CHOH$. Above 200 K, the singlet of the $•SO_2NHTf$ radical appears (SI Figure 20S), but the reduced signal from the persistent radical is still observed, as shown in the plot. No signals from $Me_3N^{+•}$ radical cations were observed in Chol NTf_2, whereas this species gives the predominant contribution to EPR spectra observed at 300 K either in Chol Cl that is irradiated at 77 K and annealed at 300 K (SI Figure 14S) or the samples that are irradiated at 300 K (Figure 3).

That the $Me_3N^{+•}$ radical cations are observed only in Chol Cl samples annealed over 250 K (i.e., after considerable thermal activation) agrees with the notion that these radicals are generated from $Me_3N^+CH_2•CHOH$ radicals in secondary reactions (such as reactions 1 or 14), but the very observation of this presumably very reactive species in room-temperature samples poses a question whether reaction 2 can indeed sustain a rapid chain reaction. In irradiated Chol NTf_2, even during *slow* warming of the sample the $Me_3N^+CH_2•CHOH$ radical cations appear to decay via recombination and/or disproportionation *before* they undergo reaction 1 or 14, i.e., the stability of these radicals in the IL parallels their reported stability in aqueous and alcohol solutions (section 2.3). If the mechanism for radiation hypersensitivity is indeed reactions 1−3, this excludes ILs, because reaction 1 is too slow to compete with other reactions of this chain-initiating radical.

Our EPR experiments provided no evidence for trapped $Me_3N^{+•}...•CH_2CH_2OH$ pairs (presumably from reaction 5) that was reported by Tomkiewicz et al.[38]

4.2.2. Pulse Radiolysis—Transient Optical Spectroscopy. Figure 7 shows TA spectra obtained from electron pulse radiolysis measurements at LEAF. For consistency, the kinetic data at each wavelength were fitted to a double exponential decay with rate constants of 2.2×10^7 and 6.1×10^6 s^{-1} (see Figure 8) which were determined by averaging fitted rate constants at several wavelengths. The resulting values fit well over the whole TA spectrum. After the solvated electron in Chol NTf_2 is consumed (>500 ns), there is a residual absorbance appearing as a shoulder between 300 and 400 nm in Figure 7 (trace iii) very similar to that observed in the radiolysis of tri(*n*-butyl)methylammonium bistriflimide.[82] Decay of the solvated electron spectrum is represented by both exponential terms, as an approximation of the effects of inhomogeneous kinetics and adventitious scavenging (see below). The minor shift in peak wavelength between the initial and intermediate spectra (traces i and ii in Figure 7) is due to an absorbance contribution to the faster decay process from a transient species related to the NTf_2^- anion, as previously mentioned in refs 82 and 109. Therefore, the intermediate spectrum with the final spectrum subtracted (trace iv in Figure 7) is the best representation of the spectrum of the solvated electron in Chol NTf_2, with a maximum around 630−640 nm. An increase in solvated electron absorption toward the UV limit

dx.doi.org/10.1021/jp5049716 | J. Phys. Chem. B 2014, 118, 10477−10492

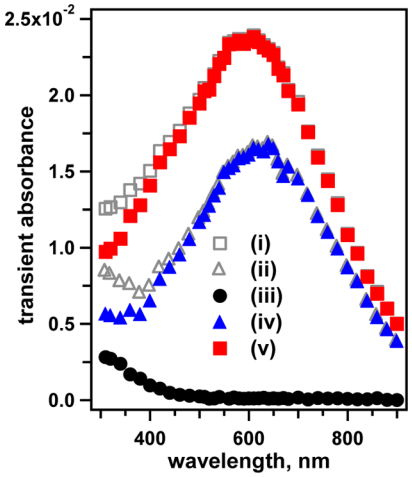

Figure 7. TA spectra collected during pulse radiolysis of Chol NTf_2 at 45 °C, normalized to a dose of 23 Gy/pulse. Traces i–iii are initial, intermediate, and final absorbances, respectively, according to the double exponential fit described in the text. Traces iv and v are traces ii and i that were corrected by subtracting the residual absorbance (trace iii).

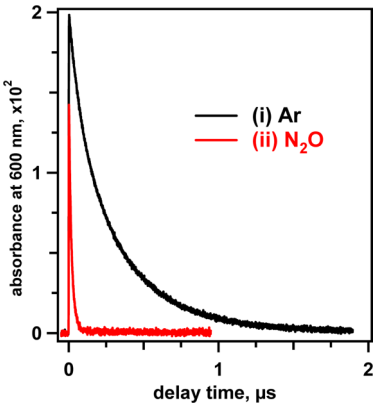

Figure 8. Pulse radiolysis TA kinetics at 600 nm of Chol NTf_2 saturated with argon (i) and N_2O (ii), which serves as an electron scavenger. Dose 19.4 Gy/pulse in the supercooled liquid at 22 °C.

of the spectrum has been observed in other ionic liquids,[82,110–112] water,[113] and liquid ammonia.[114]

The absorption spectrum of the solvated electron in Chol NTf_2 has a peak around 630–640 nm that is typical of solvated electrons in alcohol solvents, e.g., methanol 636 nm,[115] ethanol 700 nm,[115] ethylene glycol and propanediols 565–575 nm,[116] and other quaternized ammonium ionic liquids with alcohol functionalities (650 nm).[111] The solvated electron in Chol NTf_2 has an average lifetime of 270–300 ns under argon at 22 °C but the lifetime is only 18 ns if the IL is saturated with N_2O, which reacts with the solvated electron (traces i and ii in Figure 8). Whereas the electron decay in saturated N_2O was single exponential, the decay under argon could be approximated by two exponentials, as mentioned above. This is typical of relatively clean ILs where the solvated electron decay process is a combination of geminate recombination and electron capture by adventitious scavengers.[117]

Pulse radiolysis transient infrared absorption spectroscopy was performed on Chol NTf_2 to look for the formation of molecular products during choline radiolysis. Prompt formation of acetaldehyde (MeCHO) and vinyl alcohol (CH_2CHOH) can result from N–C bond scission through excited state or radical pathways, reaction 4. The frequency of the C=O stretching vibration of acetaldehyde in Chol NTf_2 was determined to be centered at 1733 cm^{-1} by static Fourier-transform infrared (FTIR) spectroscopy. Vinyl alcohol is unstable with respect to tautomerization into acetaldehyde; however, the conversion is slow in the absence of catalysis by excess protons.[118,119] Nonetheless, due to the instability of vinyl alcohol it was not practical to determine the frequency of its C=C stretch in Chol NTf_2 by static FTIR. Instead, it was estimated by analogy from its observed frequency of 1639 cm^{-1} in irradiated CO_2/ethylene ice at 10 K.[120] Under the same conditions the C=O stretch of acetaldehyde appeared at 1723 cm^{-1};[120] therefore, the region around 1649 cm^{-1} was examined for evidence of an absorption band and one was indeed found between 1644 and 1668 cm^{-1}. The integrated absorption coefficients of both tautomers in irradiated CO_2/ethylene ice at 10 K are roughly equivalent[120] and we will assume that the same holds in Chol NTf_2.

The rise time of the IR detection system is on the order of 40 ns, and within that time we observe prompt formation of both acetaldehyde and vinyl alcohol in approximately equal amounts. No evolution of either tautomer occurs on the time scale of the solvated electron decay (<500 ns at 50 °C). On the time scale of 0.45 ms (traces i and ii in Figure 9) the absorbance of vinyl

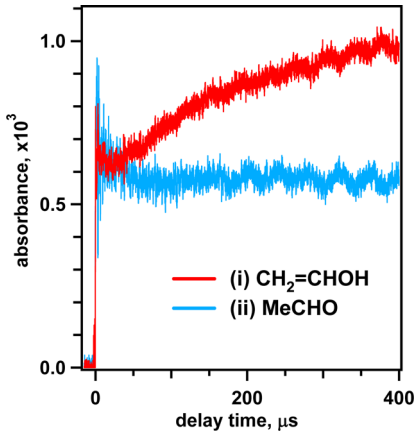

Figure 9. Pulse radiolysis infrared transient absorption kinetics of Chol NTf_2 saturated with argon at 50 °C. Dose 430 Gy/pulse. Traces i and ii correspond to C=C and C=O vibrational bands in vinyl alcohol (1649 cm^{-1}) and acetaldehyde (1733 cm^{-1}), respectively.

alcohol increases by about 40% with a rate constant of 5500 s^{-1}, after an induction period. No further changes are seen out to 1 s. Our results suggest that most of the radiolytically induced C_1–N fragmentation in Chol NTf_2 occurs promptly (most likely, in reaction 4 of the electronically excited cation or via DEA reaction 12, except involving presolvated electron states). The very slow formation of the enol from "persistent radical" cation $Me_3N^+CH_2{}^\bullet$CHOH that escapes spur recombination (reaction 1) suggests that Symons' mechanism based on the notion of rapid and efficient chain propagation is certainly incorrect. This inefficiency was also apparent from our EPR results discussed in section 4.2.1.

It is possible to make rough estimates for radiolytic yields of the fragmentation products in Figure 9, assuming initial absorbances at 1649 and 1733 cm^{-1} of 6×10^{-4} and a final absorbance of 10^{-3} at 1733 cm^{-1}. We shall use our measured extinction coefficient for acetaldehyde (189 M^{-1} cm^{-1}) and

dx.doi.org/10.1021/jp5049716 | J. Phys. Chem. B 2014, 118, 10477–10492

estimate that of vinyl alcohol by the ratio of integrated absorption coefficients given in Table 3 of ref 120 (2.8×10^{-17} and 3.0×10^{-17} cm/molecule for vinyl alcohol and acetaldehyde, respectively). The resulting yields are 0.67 molecules/100 eV for acetaldehyde and 0.72 and 1.2 molecules/100 eV for the prompt and final yields of vinyl alcohol, respectively.

4.3. Carnitinium Compounds. Hcar Cl (like Chol Cl and Hbet Cl) has been reported to exhibit higher-than-usual decomposition rates in radiolysis (SI Table 1S), but unlike Chol Cl, it has not been studied spectroscopically. SI Figure 21S(a) demonstrates the EPR spectrum of irradiated Hcar Cl. This EPR spectrum is composite, as can be demonstrated through a gradual decrease in the intensity of the two side lines indicated by the arrows between 50 and 150 K (Figure 10); the

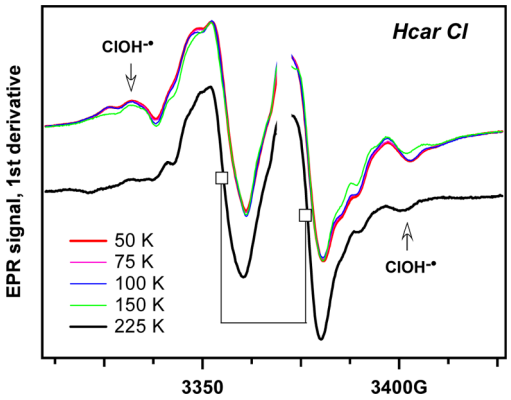

Figure 10. First-derivative EPR spectra of Hcar Cl irradiated at 77 K observed at 50−225 K. The side lines indicated by arrows are from the $ClOH^{-\bullet}$ radical anion. This species decays above 175 K, and the resulting doublet (indicated by vertical lines and open squares) persists to 300 K. We attribute this feature to the $Me_3N^+CH_2CH(OH)^\bullet CHCO_2H$ radical cation.

residual signal is a doublet indicated by the open squares in Figure 10. Around the same temperature, the resonance lines of the $Cl_2^{-\bullet}$ radical anion also appear (SI Figure 21S(b)). The disappearing set of lines is from the $ClOH^{-\bullet}$ radical that is also observed in irradiated Chol Cl.[40] The doublet signal persists even at 300 K (SI Figures 14S and 22S), where the resonance line overlaps with the multiplet of $Me_3N^{+\bullet}$ radical cation.

In irradiated Hcar NTf_2 (SI Figure 23S(a)), in addition to the familiar $^\bullet CF_2X$ radicals there is also a doublet analogous to the one observed in Hcar Cl. The EPR spectrum of this species does not change between 50 and 150 K (SI Figure 24S). At higher temperature, the resonance line of the $^\bullet SO_2NHTf$ radical overlaps with this doublet signal, but the latter can still be observed until the matrix softens at 225 K (SI Figure 23S(b)).

That the persistent radical appears as a doublet excludes all of the $^\bullet CH_2R$ radicals that are generated via decarboxylation or deamination, as these radicals would have two coupled $^1H_\alpha$ nuclei with $a_{iso} \sim -23$ G (SI Tables 4S and 5S). For the same reason we can exclude from consideration the $Me_3N^+CH_2^\bullet C(OH)CH_2CO_2H$ radical cation, as in this species at least two of the $^1H_\beta$ nuclei would *always* have nonzero hfcc's. This leaves a choice between the $Me_3N^{+\bullet}CHCH(OH)CH_2CO_2H$ and $Me_3N^+CH_2CH(OH)^\bullet CHCO_2H$ radical cations that assumed a conformation in which $a_{iso}(^1H_\beta) \sim 0$. Our DFT calculations suggest that the C−H bond energy is considerably lower for carbon-3 (Scheme 1 and SI Table 8S), suggesting that it is the latter radical cation (a similar preference is observed for choline and many amino acids). Another computational result is that in the gas phase this radical has almost the same energy as $Me_3N^{+\bullet}$ + $MeC(O)CH_2CO_2H$ (SI Table 8S), suggesting that it can be the progenitor of the $Me_3N^{+\bullet}$ radical cations upon thermal activation (as was observed experimentally in the Hcar Cl crystal)

$$\{Me_3N^+CH_2CH(OH)^\bullet CHCO_2H\}A^- \rightarrow Me_3N^{+\bullet}A^- + MeC(O)CH_2CO_2H \quad (18)$$

which is analogous to reaction 14. Furthermore, in the gas phase the energy of this carbon-3 centered radical is 40 meV greater than $Me_3N^+CH_2CH(OH)^\bullet CH_2 + CO_2$ (whereas for the $Me_3N^{+\bullet}CHCO_2H$ radical cation, CO_2 elimination is strongly endergonic, see section 4.1 and SI Table 7S). This may explain why the decarboxylation reaction 9b is the preferred oxidation pathway for betainium but not for carnitinium, which instead undergoes reaction 6.

In all of these systems, gas-phase energetics proved to be surprisingly good in predicting the observed reaction preferences.

5. DISCUSSION

From the standpoint of the *primary* chemistry, the cations shown in Scheme 1 proved to be quite similar to other organic cations that we studied. Radiolytic oxidation preferentially follows the most exergonic route, which is the decarboxylation for betaine and H loss from carbon-2 for choline and carbon-3 for carnitinium, respectively (Scheme 1). These reactions occur in both the crystalline chloride and frozen bistriflimide IL compounds. In the latter, there is no evidence for reductive deamination by *solvated* electrons, although presolvated electrons may induce deamination (reaction 12) in competition with the solvation process and with DEA to the NTf_2^- anion (reaction 17). For betainium chloride, there is indirect evidence for deamination in the chloride compound (that also occurs in other α-amino acids). For choline and carnitinium, we failed to observe this reaction at all, contrary to the previous claims (section 2.2). The latter can be due to the preferential electron trapping by hydroxyl and/or carboxylic acid groups and the resulting $H^\bullet$ atom formation (reaction 11). The released $H^\bullet$ atoms abstract H from the parent cation and the resulting radicals are the same as the one generated in the oxidation channel. Our TRIR kinetic measurements indicate rapid (<40 ns) formation of acetaldehyde and vinyl alcohol through excited state chemistry (reaction 4) or dissociative attachment of presolvated electrons (reaction 12). We obtained direct spectroscopic evidence for the formation of metastable solvated electrons in choline compounds, whose disappearance apparently does not proceed through reaction 12 because there is no concurrent increase in the IR signal of vinyl alcohol or acetaldehyde on the time scale of electron decay. This is consistent with previous reports on the radiolysis of quaternary ammonium ionic liquids.

For betaine, there is some prompt C−N bond homolysis in an excited state, although the yield of this reaction is low; for choline and carnitine, no such dissociation is observed and the $Me_3N^{+\bullet}$ radical cation is a product of secondary reactions, which require considerable thermal activation. This transformation was observed only in crystalline compounds.

dx.doi.org/10.1021/jp5049716 | J. Phys. Chem. B 2014, 118, 10477−10492

Our identification of the persistent radical in irradiated α-Chol Cl as the lowest energy conformer of the $Me_3N^+CH_2^•CHOH$ radical (rather than β-hydroxyethyl radical) suggests that even in this crystal, the dissociation of this radical is quite inefficient. Figure 9 indicates just how slow the C−N bond scission is in this radical cation in room-temperature radiolysis of Chol NTf_2. Furthermore, the $Me_3N^{+•}$ radical cation seems to be surprisingly stable in all three of the chloride crystals that we studied.

Can Symons' mechanism account for these new results? Our experimental evidence points to the stability of the $Me_3N^+CH_2^•CHOH$ radical cation in the α-Chol Cl matrix when the latter assumes the same lowest-energy conformation that it assumes in the solution. This is indicated by the similarity of the hfcc's for the trapped (persistent) radical in the crystal and free radicals in solution. This conformation is also almost the same as the one for the parent cation in the α-polymorph. As suggested by our DFT calculations (section 2.3), the C_1−N bond scission in this species can occur only when this bond and the C_2−O bond are nearly in the same plane, which requires thermal activation of a fraction of an electronvolt. The important point is that such a reaction would be slow on the usual time scale for radical reactions, and this is also directly suggested by TRIR results. The "magic" of α-Chol Cl appears to be less in *catalysis* of reaction 1 or 14 than in *isolation* of the $Me_3N^+CH_2^•CHOH$ radical cations, giving this species ample time to decompose before it reacts with other radicals. Likewise, the resulting $Me_3N^{+•}$ radical cations are not particularly reactive. That was the case not only for choline chloride, but also for betainium and carnitinium chlorides (section 3). However, once again, in α-Chol Cl, these fragment radical cations are so isolated that reaction 2 occurs nevertheless, propagating the chain.

We reach an important conclusion. The peculiarity of α-Chol Cl is less in that it can sustain a rapid radical chain reaction than the extreme inefficiency of chain termination in this system. For energetic β and γ particles with energies of 0.1−100 MeV, the energy deposition along the track occurs in clusters of 1−5 ionization events called spurs; these spurs are spatially isolated, so interspur radical reactions require mobility of the species that are formed in the spurs. A suppression of these intra- and interspur reactions would require very diffuse spurs, exceptionally slow diffusion of radical (ions), or unusually inefficient cross recombination reactions—or the confluence of these three factors.

This brings us to another insight reached in section 4. For every trapped-hole species (like the $Me_3N^+CH_2^•CHOH$ radical cation), there should be a trapped-electron species. When the persistent radical was believed to be β-hydroxyethyl radical, electron trapping in α-Chol Cl was assumed to be reaction 3. However, we demonstrated that this reaction does not occur. The excess electrons are either trapped collectively by hydroxyl groups (assisted by the positive head groups) yielding solvated/trapped electrons or react with the $H^{\delta+}A^{\delta-}$ species (most likely, $\{Me_3N^+CH_2CH_2OH_2^+\}Cl^-$ pairs) that are formed in reaction 6. In both cases, proton transfer reactions 12 and 19 release mobile $H^•$ atoms.

$$H^{\delta+}A^{\delta-} + e^{-•} \rightarrow H^• + A^- \quad (19)$$

These $H^•$ atoms would migrate out and abstract H from the parent cation yielding the same $Me_3N^+CH_2^•CHOH$ radicals

$$H^• + Me_3N^+CH_2CH_2OH \rightarrow Me_3N^+CH_2^•CHOH + H_2 \quad (20)$$

In this regard, it is not surprising that choline-containing ionic crystals that include electron-scavenging anions are not hypersensitive, as the electron attachment to these anions causes the formation of compact spurs, where cross recombination can outcompete chain propagation. Thus, incorporation of nitrate, acetate, or acetyl groups dramatically reduces radiation sensitivity (SI Table 1S). With anions that do not trap electrons (like sulfate and (pseudo)halide anions), electron localization presumably occurs at the sites of anion vacancies (as occurs in alkali halide crystals). In α-Chol Cl, the chloride ion forms an H bond with one of the hydroxyl groups in the $Chol^+$ cations,[121] and this anion is surrounded by four trimethylammonium groups (SI Scheme 2S). In an anion vacancy, two cations would rotate hydroxyl groups toward the center in order to minimize repulsion between the positively charged head groups; such anion vacancies would be ideal for electron trapping in the crystal (which is known to occur in carbohydrate crystals).[80,81] We know that electron solvation occurs in Chol NTf_2 (section 4.2.2) and there are many indirect indications that the electron trapping also occurs in the crystal (section 2.1). The $H^•$ atom diffusion preceding reaction 20 can contribute to increasing the average distance between the persistent $Me_3N^+CH_2^•CHOH$ radicals in irradiated α-Chol Cl. However, in itself this is only a contributing factor.

We suggest that the main peculiarity of this system is the interplay of radical chemistry with the crystal structure. As has been noticed by Foster and co-workers,[36] in α-Chol Cl, the cations form a chain along crystallographic axis *c*, as shown in SI Scheme 2S. The cations in this chain are aligned along the crystallographic axis, but the direction of the alignment alternates from one chain to another. If reaction 2 occurs only in a preferred direction along the chain (as this minimizes the distance between the secondary $Me_3N^{+•}$ radical cation and the C_2−H bond), reactions 1 and 2 would propagate either in the direction along axis *c* or in the opposite direction, depending on the orientation of the chain that contains the initial radical (Figure 11a). If interchain reaction 2 is suppressed and the diffusion/propagation of the "persistent radical" (that is $Me_3N^+CH_2^•CHOH$) from one chain to another is inhibited, the radical chain propagation becomes confined to these cation chains (Figure 11a). Statistically, either direction of the radical chain propagation is possible, so for every ionization event, one-half of these events would yield a pair of the $Me_3N^+CH_2^•CHOH$ radical cations that propagate in opposite directions (confined to their respective cation chains), as shown in Figure 11a,b. Cross recombination of such radical species would be a low probability event involving the radicals propagating from other spurs. This allows the radical chain to propagate for a long period of time before termination. In other words, the combination of preferential radical chain propagation and suppressed interchain diffusion would sustain the radical chain even when the reactions responsible for this propagation are slow.

In a molecular medium, Coulomb interaction of ionized molecules causes efficient cross recombination of radical ions. This is not the case in radiolysis of the α-Chol Cl. The radical cations (having the same net charge as the original choline cations) propagate in the opposite directions along axis *c*. Left to recombine near the original locus of the spur are neutral species (such as Me_3N), protonated choline cation (reaction 6),

dx.doi.org/10.1021/jp5049716 | J. Phys. Chem. B 2014, 118, 10477−10492

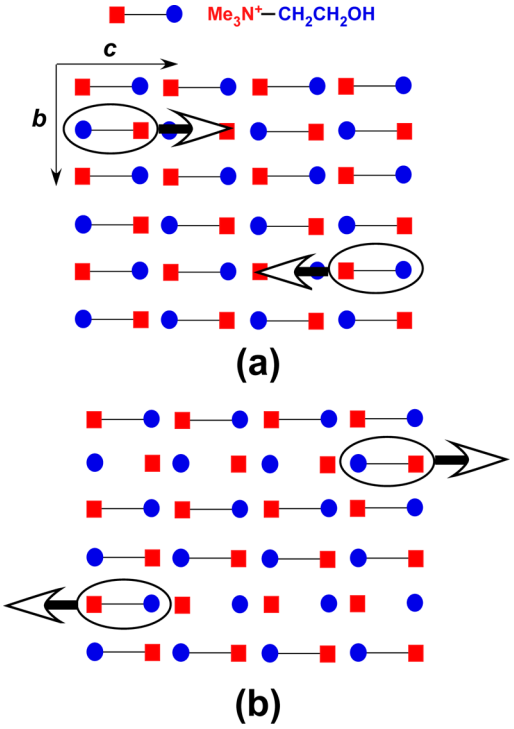

Figure 11. Suggested mechanism for radiation hypersensitivity in α-Chol Cl. A layer composed of the cation chains oriented along axis c is viewed along axis a of the crystal. There are two such layers per unit cell. In the initial stage (a), two $Me_3N^+CH_2{}^\bullet CHOH$ radical cations generated in the same spur belong to two cation chains that are aligned in the opposite directions along crystallographic axis c of this crystal. In the secondary stage (b), the radicals propagate via reactions 2 and 14 along the cation chain in the directions indicated with the bold arrows. As chain-to-chain migration of radicals is largely suppressed, these radicals quickly separate through this propagation so much that their cross recombination and disproportionation become insignificant.

and uncompensated Cl^- anion (after reaction 12); these species eventually combine to yield Me_3NH^+ Cl^- pairs. The recombination of these residual species has no bearing on the radical chain propagation. When the α-polymorph crystal undergoes high-temperature transition to the β-polymorph,[39,41] this ordered cation-chain structure favoring coaxial propagation of the radical chain reaction becomes disrupted,[48−50] and the radical chain propagation loses its directionality and the radical chains quickly terminate.

The above consideration suggests that directional radical chain propagation in a crystal would explain the observed peculiarities of radiation hypersensitivity, but it does not specify the origin of such extreme stereoselectivity. An examination of the crystal structure for α-Chol Cl indicates that the distances between N atoms of one choline and methylene hydrogens of another are much shorter (5.5 Å vs >8.5 Å) along the cation chain containing the original choline cation than in any other direction. Since these cation chains are isolated by anion chains, the released $Me_3N^{+\bullet}$ radical cations (Figure 12) are trapped in their original site, and the closest approach for abstraction of an H atom is toward the "tail" of another cation in the chain, as shown in Figure 12. The H atom abstraction (reaction 2) can be direct (reaction pathway 1 in Figure 12) or a concerted reaction that involves abstraction of the hydroxyl proton and 1,2-shift (reaction pathways 2a and 2b in Figure 12). Clearly, this uncommon solid phase radical reaction would merit a thorough computational study, detailing energetics of such stereo preference.

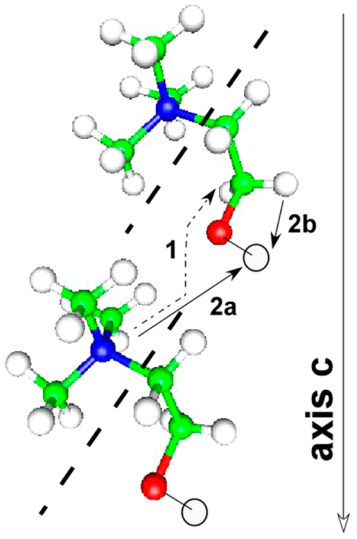

Figure 12. Sketch of stereoselective radical chain propagation along axis c in the α-polymorph of Chol Cl. Loci for H atom abstraction by the $Me_3N^{+\bullet}$ radical cation fragment of choline are indicated in the sketch.

6. CONCLUDING REMARKS

In this study, matrix isolation EPR spectroscopy and pulse radiolysis−optical spectroscopy methods have been used to address two pivotal issues in the radiation chemistry of liquid and solid compounds consisting of functionalized organic cations. Both of these issues have direct bearing on the potential of task-specific ionic liquids (TSILs) and related eutectic mixtures as unique solvents in wet processing of spent nuclear fuel, which exposes these diluents to high-dose ionizing radiation. The first issue is the nature of radiation hypersensitivity in crystals consisting of such functionalized organic ions; this has been an open problem for 60+ years. The second issue is the radiation stability of TSILs that are based on cations whose crystalline analogues exhibit this radiation hypersensitivity.

Our general conclusion is that radiation hypersensitivity is the extreme case of a stereoselection effect in radical chain reactions occurring in highly ordered crystals; as such, this detrimental phenomenon cannot and does not occur in ionic liquids and disordered solids. We show that the previously suggested model of a radical chain propagation reaction (by Martyn Symons)[36,40] as the main cause for the radiation hypersensitivity is essentially correct, yet this reaction is neither unusually rapid nor efficient, as was implied in the models. Rather, the radiation hypersensitivity is caused by unusual inefficiency of termination reactions competing with the radical chain propagation. We suggest that this property requires the confluence of several factors that are scrutinized in section 4. The most important of these factors are (i) tight stereo control of the radical reaction that causes it to propagate through cation chains without interchain hopping, (ii) initiation of two such radical chain reactions by the electron and the hole, and (iii) a specific mode of electron localization that favors intermittent electron trapping over dissociative C−N bond dissociation in the cation head groups, and (iv) low yield of radical fragmentation in the excited states. When there is no

dx.doi.org/10.1021/jp5049716 | J. Phys. Chem. B 2014, 118, 10477−10492

confluence of these factors, radical cross recombination always outruns chain propagation, and radiation sensitivity remains low. Such a situation occurs even in frozen (disordered) TSILs; even more so it occurs in the fluid. While the TSILs may exhibit radiation decomposition that is somewhat in excess of the ILs due to weaker chemical bonds involving heteroatoms, there is no reason to expect the runaway radiolytic decomposition that was discovered by Melvin Calvin and co-workers.

■ ASSOCIATED CONTENT

Supporting Information

List of abbreviations and reactions, Schemes 1S and 2S, Tables 1S to 8S, and Figures 1S to 24S with captions, including experimental and simulated EPR spectra. This material is available free of charge via the Internet at http://pubs.acs.org.

■ AUTHOR INFORMATION

Corresponding Author

*Tel. (630) 252-9516, e-mail shkrob@anl.gov.

Notes

The authors declare no competing financial interest.

■ ACKNOWLEDGMENTS

We thank D. Quigley, S. Chemerisov, Y. Portilla, B. Layne and S. Ramati for technical support. This material is based upon work supported by the U.S. Department of Energy Office of Science, Office of Basic Energy Sciences, Division of Chemical Sciences, Geosciences, and Biosciences under Award Numbers DE-AC02-06CH11357 (Argonne) and DE-AC02-98CH10886 (Brookhaven). This research used resources of the LEAF Facility of the Brookhaven Accelerator Center for Energy Research, which is a DOE Office of Science User Facility. Programmatic support via a DOE SISGR grant "An Integrated Basic Research Program for Advanced Nuclear Energy Separations Systems Based on Ionic Liquids" is gratefully acknowledged. The submitted manuscript has been created by UChicago Argonne, LLC, Operator of Argonne National Laboratory ("Argonne"). Argonne, a U.S. Department of Energy Office of Science laboratory, is operated under Contract No. DE-AC02−06CH11357. The U.S. Government retains for itself, and others acting on its behalf, a paid-up nonexclusive, irrevocable worldwide license in said article to reproduce, prepare derivative works, distribute copies to the public, and perform publicly and display publicly, by or on behalf of the Government.

■ REFERENCES

(1) Venkatesan, A. K.; Srinivasan, T. G.; Vasudeva Rao, P. R. A Review on the Electrochemical Applications of Room Temperature Ionic Liquids in Nuclear Fuel Cycle. *J. Nucl. Radiochem. Sci.* **2009**, *10*, R1−R6.

(2) Ha, S. H.; Menchavez, R. N.; Koo, Y.-M. Reprocessing of Spent Nuclear Waste Using Ionic Liquids. *Korean J. Chem. Eng.* **2010**, *27*, 1360−1365.

(3) Sun, X. Q.; Luo, H. M.; Dai, S. Ionic Liquids-Based Extraction: A Promising Strategy for the Advanced Nuclear Fuel Cycle. *Chem. Rev.* **2012**, *112*, 2100−2128.

(4) Kolarik, Z. Ionic Liquids: How Far Do They Extend the Potential of Solvent Extraction of f-Elements? *Solv. Extr. Ion Exch.* **2013**, *31*, 24−60.

(5) Shkrob, I. A.; Marin, T. W.; Hatcher, J. L.; Cook, A. R.; Szreder, T.; Wishart, J. F. Radiation Stability of Cations in Ionic Liquids. 2. Improved Radiation Resistance through Charge Delocalization in 1-Benzylpyridinium. *J. Phys. Chem. B* **2013**, *117*, 14385−14399.

(6) Shkrob, I. A.; Marin, T. W.; Luo, H.; Dai, S. Radiation Stability of Cations in Ionic Liquids. 1. Alkyl and Benzyl Derivatives of 5-Membered Ring Heterocycles. *J. Phys. Chem. B* **2013**, *117*, 14372−14384.

(7) Shkrob, I. A.; Marin, T. W.; Luo, H.; Dai, S. Radiation Stability of Cations in Ionic Liquids. 3. Cyclical Guanidinium Cations. *J. Phys. Chem. B* **2013**, *117*, 14400−14407.

(8) Shkrob, I. A.; Marin, T. W. Radiation Stability of Cations in Ionic Liquids. 4. Task-Specific Antioxidant Cations for Nuclear Separations and Photolithography. *J. Phys. Chem. B* **2013**, *117*, 14797−14807.

(9) Visser, A. E.; Swatloski, R. P.; Reichert, W. M.; Mayton, R.; Sheff, S.; Wierzbicki, A.; Davis, J. H.; Rogers, R. D. Task-Specific Ionic Liquids for the Extraction of Metal Ions from Aqueous Solutions. *Chem. Commun.* **2001**, 135−136.

(10) Davis, J. H. Task-Specific Ionic Liquids. *Chem. Lett.* **2004**, *33*, 1072−1077.

(11) Lee, S. Functionalized Imidazolium Salts for Task-Specific Ionic Liquids and Their Applications. *Chem. Commun.* **2006**, 1049−1063.

(12) Nockemann, P.; Thijs, B.; Pittois, S.; Thoen, J.; Glorieux, C.; Van Hecke, K.; Van Meervelt, L.; Kirchner, B.; Binnemans, K. Task-Specific Ionic Liquid for Solubilizing Metal Oxides. *J. Phys. Chem. B* **2006**, *110*, 20978−20992.

(13) Ouadi, A.; Gadenne, B.; Hesemann, P.; Moreau, J. J. E.; Billard, I.; Gaillard, C.; Mekki, S.; Moutiers, G. Task-Specific Ionic Liquids Bearing 2-Hydroxybenzylamine Units: Synthesis and Americium-Extraction Studies. *Chem.—Eur. J.* **2006**, *12*, 3074−3081.

(14) Nockemann, P.; Thijs, B.; Parac-Vogt, T. N.; Hecke, K. V.; Van Meervelt, L.; Tinant, B.; Hartenbach, I.; Schleid, T.; Ngan, V. T.; Nguyen, M. T.; et al. Carboxyl-Functionalized Task-Specific Ionic Liquids for Solubilizing Metal Oxides. *Inorg. Chem.* **2008**, *47*, 9987−9999.

(15) Nockemann, P.; Thijs, B.; Van Hecke, K.; Van Meervelt, L.; Binnemans, K. Polynuclear Metal Complexes Obtained from the Task-Specific Ionic Liquid Betainium Bistriflimide. *Cryst. Growth Design* **2008**, *8*, 1353−1363.

(16) Fagnant, J. D. P.; Goff, G. S.; Scott, B. L.; Runde, W.; Brennecke, J. F. Switchable Phase Behavior of [Hbet][Tf_2N]−H_2O Upon Neodymium Loading: Implications for Lanthanide Separations. *Inorg. Chem.* **2013**, *52*, 549−551.

(17) Chen, X.-Y.; Goff, G. S.; Quiroz-Guzman, M.; Fagnant, J. D. P.; Brennecke, J. F.; Scott, B. L.; Runde, W. Directed Nucleation of Monomeric and Dimeric Uranium(VI) Complexes with a Room Temperature Carboxyl-Functionalized Phosphonium Ionic Liquid. *Chem. Commun.* **2013**, *49*, 1903−1905.

(18) Binnemans, K. Lanthanides and Actinides in Ionic Liquids. *Chem. Rev.* **2007**, *107*, 2592−2614.

(19) Nockemann, P.; Binnemans, K.; Thijs, B.; Parac-Vogt, T. N.; Merz, K.; Mudring, A.-V.; Menon, P. C.; Rajesh, R. N.; Cordoyiannis, G.; Thoen, J.; et al. Temperature-Driven Mixing-Demixing Behavior of Binary Mixtures of the Ionic Liquid Choline Bis-(Trifluoromethylsulfonyl)Imide and Water. *J. Phys. Chem. B* **2009**, *113*, 1429−1437.

(20) Nockemann, P.; Van Deun, R.; Thijs, B.; Huys, D.; Vanecht, E.; Van Hecke, K.; Van Meervelt, L.; Binnemans, K. Uranyl Complexes of Carboxyl-Functionalized Ionic Liquids. *Inorg. Chem.* **2010**, *49*, 3351−3360.

(21) Vander Hoogerstraete, T.; Onghena, B.; Binnemans, K. Homogeneous Liquid−Liquid Extraction of Metal Ions with a Functionalized Ionic Liquid. *J. Phys. Chem. Lett.* **2013**, *4*, 1659−1663.

(22) Vander Hoogerstraete, T.; Onghena, B.; Binnemans, K. Homogeneous Liquid−Liquid Extraction of Rare Earths with the Betaine—Betainium Bis(Trifluoromethylsulfonyl)Imide Ionic Liquid System. *Int. J. Mol. Sci.* **2013**, *14*, 21353−21377.

(23) Shkrob, I. A.; Marin, T. W.; Jensen, M. P. Ionic Liquid Based Separations of Trivalent Lanthanide and Actinide Ions. *Ind. Eng. Chem. Res.* **2014**, *53*, 3641−3653.

(24) Dai, Y.; van Spronsen, J.; Witkamp, G.-J.; Verpoorte, R.; Choi, Y. H. Ionic Liquids and Deep Eutectic Solvents in Natural Products

Research: Mixtures of Solids as Extraction Solvents. *J. Nat. Prod.* **2013**, *76*, 2162−2173.
(25) Abbott, A. P.; Boothby, D.; Capper, G.; Davies, D. L.; Rasheed, R. K. Deep Eutectic Solvents Formed between Choline Chloride and Carboxylic Acids: Versatile Alternatives to Ionic Liquids. *J. Am. Chem. Soc.* **2004**, *126*, 9142−9147.
(26) Tsuda, T.; Boyd, L. E.; Kuwabata, S.; Hussey, C. L. Electrochemistry of Copper(I) Oxide in the 66.7−33.3 Mol % Urea-Choline Chloride Room-Temperature Eutectic Melt. *J. Electrochem. Soc.* **2010**, *157*, F96−F103.
(27) Abbott, A. P.; Capper, G.; Davies, D. L.; Rasheed, R. K.; Shikotra, P. Selective Extraction of Metals from Mixed Oxide Matrixes Using Choline-Based Ionic Liquids. *Inorg. Chem.* **2005**, *44*, 6497−6499.
(28) Curto, V. F.; Scheuermann, S.; Owens, R. M.; Ranganathan, V.; MacFarlane, D. R.; Benito-Lopez, F.; Diamond, D. Probing the Specific Ion Effects of Biocompatible Hydrated Choline Ionic Liquids on Lactate Oxidase Biofunctionality in Sensor Applications. *Phys. Chem. Chem. Phys.* **2014**, *16*, 1841−1849.
(29) Lindblom, R. O.; Lemmon, R. M.; Calvin, M. Kinetic and Electron Spin Resonance Studies of the Radiation Decomposition of Crystalline Choline Chloride. *J. Am. Chem. Soc.* **1961**, *83*, 2484−2489.
(30) Lemmon, R. M.; Parsons, M. A.; Chin, D. M. Effects of Ionizing Radiation on Choline Chloride and Its Analogs. *J. Am. Chem. Soc.* **1955**, *77*, 4139−4142.
(31) Serlin, I. Thermal Protection of Choline Chloride from Decomposition by Ionizing Radiation. *Science* **1957**, *126*, 261.
(32) Collin, R. L. Polymorphism and Radiation Decomposition of Choline Chloride. *J. Am. Chem. Soc.* **1957**, *79*, 6086−6086.
(33) Lemmon, R. M.; Gordon, P. K.; Parsons, M. A.; Mazzetti, F. Effects of Ionizing Radiation on Choline Chloride and Its Analogs. II. *J. Am. Chem. Soc.* **1958**, *80*, 2730−2733.
(34) Smith, M. A.; Lemmon, R. M. A Study of the Radical Termination Mechanisms in the Radiolysis of Crystalline Choline Chloride. *J. Phys. Chem.* **1965**, *69*, 3370−3373.
(35) Nath, A.; Agarwal, R.; Marton, L.; Subramanyan, V.; Lemmon, R. M. The Role of Detrapped Electrons in the Radiolysis of Crystalline Choline Chloride. *J. Am. Chem. Soc.* **1970**, *93*, 2103−2107.
(36) Foster, T.; West, P. R. Electron Spin Resonance Studies in Aqueous Solution: Fragmentation of Radical Intermediates Derived from Beta-Amino Alcohols. *Can. J. Chem.* **1973**, *51*, 4009−4017.
(37) Foster, T.; West, P. R. Photolysis of Aqueous Solutions of Hydrogen Peroxide Containing Beta-Ammonio Alcohols. *Can. J. Chem.* **1974**, *52*, 3589−3598.
(38) Tomkiewicz, Y.; Agarwal, R.; Lemmon, R. M. Solid-State Chemistry of Irradiated Choline Chloride. *J. Am. Chem. Soc.* **1973**, *95*, 3144−3149.
(39) Petrouleas, V.; Nath, A.; Lemmon, R. M. Phase Transitions and Radiation Sensitivity of Choline Chloride, Bromide and Iodide. *Radiat. Phys. Chem.* **1980**, *16*, 113−117.
(40) Symons, M. C. R. Unstable Intermediates. Part 107. Radiation Damage Products in Choline Chloride. *J. Chem. Soc., Faraday Trans. 2* **1972**, 216−220.
(41) Petrouleas, V.; Lemmon, R. M.; Christensen, A. X-Ray Diffraction Study of Choline Chloride's Beta Form. *J. Chem. Phys.* **1978**, *68*, 2243−2246.
(42) Senko, M. E.; Templeton, D. H. Unit Cells of Choline Halides and Structure of Choline Chloride. *Acta Crystallogr.* **1960**, *13*, 281−285.
(43) Hjortas, J.; Sorum, H. A Re-Investigation of the Crystal Structure of Choline Chloride. *Acta Crystallogr., Sect. B* **1971**, *27*, 1320.
(44) Craciun, S.; Balskus, E. P. Microbial Conversion of Choline to Trimethylamine Requires a Glycyl Radical Enzyme. *Proc. Natl. Acad. Sci. U. S. A.* **2012**, *109*, 21307−21312.
(45) Duboc-Toia, C.; Hassan, A. K.; Mulliez, E.; Ollagnier-de Choudens, S.; Fontecave, M.; Leutwein, C.; Heider, J. Very High-Field EPR Study of Glycyl Radical Enzymes. *J. Am. Chem. Soc.* **2002**, *125*, 38−39.
(46) Selmer, T.; Pierik, A. J.; Heider, J. New Glycyl Radical Enzymes Catalysing Key Metabolic Steps in Anaerobic Bacteria. *Biol. Chem.* **2005**, *386*, 981−988.
(47) Tolbert, B. M.; Adams, P. T.; Bennett, E. L.; Hughes, A. M.; Kirk, M. R.; Lemmon, R. M.; Noller, R. M.; Ostwald, R.; Calvin, M. Observations on the Radiation Decomposition of Some Carbon-14 Labeled Compounds. *J. Am. Chem. Soc.* **1953**, *75*, 1867−1868.
(48) Pratum, T. K.; Klein, M. P. A ^{2}H and ^{14}N NMR Study of Molecular Motion in Polycrystalline Choline Salts. *J. Magn. Reson.* **1989**, *81*, 350−370.
(49) Wemmer, D.; Petrouleas, V.; Panaglotopoulos, N.; Filoppakis, S. E.; Lemmon, R. M. High-Resolution Solid-State Nuclear Magnetic Resonance and X-Ray Structure Study of Choline Chloride, Bromide, and Iodide. *J. Phys. Chem.* **1983**, *87*, 999−1003.
(50) Graham, J. D.; Hannon, R. H. Spin-Lattice Relaxation, Phase Transitions, and Molecular Freedom in Choline Chloride and Iodide. *J. Magn. Reson.* **1976**, *23*, 97−101.
(51) Gilbert, B. C.; Larkin, J. P.; Norman, R. O. C. Electron Spin Resonance Studies. Part XXXIII. Evidence for Heterolytic and Homolytic Transformations of Radicals from 1,2-Diols and Related Compounds. *J. Chem. Soc. Perkin Trans. II* **1972**, 794−802.
(52) Dixon, W. T.; Norman, R. O. C.; Buley, A. L. Electron Spin Resonance Studies of Oxidation. Part II. Aliphatic Acids and Substituted Acids. *J. Chem. Soc.* **1964**, 3625−3634.
(53) Taniguchi, H.; Fukui, K.; Ohnishi, S.; Hatano, H.; Hasegawa, H.; Maruyama, T. Free-Radical Intermediates in the Reaction of the Hydroxyl Radical with Amino Acids. *J. Phys. Chem.* **1968**, *72*, 1926−1931.
(54) Box, H. C.; Budzinski, E. E.; Freund, H. G. Radical Formation in X-Irradiated Glycine HCl. *J. Chem. Phys.* **1969**, *50*, 2880−2884.
(55) Shkrob, I. A.; Marin, T. W.; Chemerisov, S. D.; Wishart, J. F. Radiation Induced Redox Reactions and Fragmentation of Constituent Ions in Ionic Liquids. 1. Anions. *J. Phys. Chem. B* **2011**, *115*, 3872−3888.
(56) Shkrob, I. A.; Marin, T. W.; Crowell, R. A.; Wishart, J. F. Photo- and Radiation- Chemistry of Halide Anions in Ionic Liquids. *J. Phys. Chem. A* **2013**, *117*, 5742−5756.
(57) Shkrob, I. A.; Wishart, J. F., Free Radical Chemistry in Room-Temperature Ionic Liquids. In *Encyclopedia of Radicals in Chemistry, Biology and Materials*; Chatgilialoglu, C., Studer, A., Eds.; John Wiley & Sons, Ltd.: Chichester, UK, 2012; pp 433−448.
(58) Shkrob, I. A.; Chemerisov, S. D.; Wishart, J. F. The Initial Stages of Radiation Damage in Ionic Liquids and Ionic Liquid-Based Extraction Systems. *J. Phys. Chem. B* **2007**, *111*, 11786−11793.
(59) Morton, J. R. Electron Spin Resonance in Irradiated Glycine Crystals. *J. Am. Chem. Soc.* **1964**, *86*, 2325−2329.
(60) Box, H. C.; Freund, H. G.; Budzinski, E. E. Paramagnetic Absorption of Irradiated Glycine. *J. Am. Chem. Soc.* **1966**, *88*, 658−660.
(61) Sevilla, M. D. Radicals Formed by the Reaction of Electrons with Amino Acids in an Alkaline Glass. *J. Phys. Chem.* **1970**, *74*, 2096−2102.
(62) Sinclair, J. ESR Study of Irradiated Glycine at Low Temperatures. *J. Chem. Phys.* **1971**, *55*, 245−251.
(63) Lassmann, G.; Damerau, W. Electron Spin Resonance of Radicals in X-Irradiated Single Crystals of N-Substituted Amino Acids. *Mol. Phys.* **1971**, *21*, 555−561.
(64) Bonifacic, M.; Stefanic, I.; Hug, G. L.; Armstrong, D. A.; Asmus, K.-D. Glycine Decarboxylation: The Free Radical Mechanism. *J. Am. Chem. Soc.* **1998**, *120*, 9930−9940.
(65) Stefanic, I.; Bonifacic, M.; Asmus, K.-D.; Armstrong, D. A. Absolute Rate Constants and Yields of Transients from Hydroxyl Radical and H Atom Attack on Glycine and Methyl-Substituted Glycine Anions. *J. Phys. Chem. A* **2001**, *105*, 8681−8690.
(66) Stefanic, I.; Ljubic, I.; Bonifacic, M.; Sabljic, A.; Asmus, K.-D.; Armstrong, D. A. A Surprisingly Complex Aqueous Chemistry of the Simplest Amino Acid. A Pulse Radiolysis and Theoretical Study on H/D Kinetic Isotope Effects in the Reaction of Glycine Anions with Hydroxyl Radicals. *Phys. Chem. Chem. Phys.* **2009**, *11*, 2256−2267.

(67) Pauwels, E.; De Cooman, H.; Waroquier, M.; Holec, E. O.; Sagstuen, E. Solved? The Reductive Radiation Chemistry of Alanine. *Phys. Chem. Chem. Phys.* **2014**, *16*, 2475−2482.
(68) Serdobov, M. V.; Symons, M. C. R. Unstable Intermediates. Part CXXXIV. Electron Spin Resonance Studies of Positive Hole Centres in Gamma-Irradiated Glycine. *J. Chem. Soc., Perkin Trans. 2* **1973**, 1808−1810.
(69) Jay-Gerin, J.-P.; Ferradini, C. Electron Solvation in Polar Liquids. In *Excess Electrons in Dielectric Media*; Ferradini, C., Jay-Gerin, J.-P., Eds.; CRC Press: Boca Raton, 1991; pp 259−285.
(70) Kevan, L. Trapped Electrons in Organic Glasses. *Adv. Radiat. Chem.* **1974**, *4*, 181−305.
(71) Schwartz, R. N.; Bowman, M. K.; Kevan, L. Matrix Proton ENDOR Studies of the Overlap of Trapped Electron Wavefunctions with First Solvation Shell Molecules in Methanol Glass at 77 K. *J. Chem. Phys.* **1974**, *60*, 1690−1691.
(72) Bales, B. L.; Kevan, L. On the Solvation of the Trapped Electron in Gamma-Iradiated Deuterated Ethanol Glass at 4 K. *J. Chem. Phys.* **1974**, *60*, 710−711.
(73) Narayana, M.; Kevan, L.; Samskog, P. O.; Lund, A.; Kispert, L. D. Electron Spin Echo Modulation Studies of the Structure of Solvated Electrons in Ethylene Glycol Glass. *J. Chem. Phys.* **1984**, *81*, 2297−2299.
(74) Ogasawara, M. Excess Electrons in Polar Matrices. In *Excess Electrons in Dielectric Media*; Ferradini, C., Jay-Gerin, J.-P., Eds.; CRC Press, Inc.: Boca Raton, 1991; pp 288−314.
(75) Rice, S. A.; Kevan, L. Comparison of Photoconductivity and Optical Spectra for Trapped Electrons in Aqueous and Alcoholic Glasses at 4.2 K. *J. Chem. Phys.* **1979**, *70*, 18−25.
(76) Soroushian, B.; Lampre, I.; Belloni, J.; Mostafavi, M. Radiolysis of Silver Ion Solutions in Ethylene Glycol: Solvated Electron and Radical Scavenging Yields. *Radiat. Phys. Chem.* **2005**, *72*, 111−118.
(77) Soroushian, B.; Lampre, I.; Bonin, J.; Pernot, P.; Pommeret, S.; Mostafavi, M. Solvation Dynamics of the Electron Produced by Two-Photon Ionization of Liquid Polyols. 1. Ethylene Glycol. *J. Phys. Chem. A* **2006**, *110*, 1705−1717.
(78) Bonin, J.; Lampre, I.; Pernot, P.; Mostafavi, M. Solvation Dynamics of Electron Produced by Two-Photon Ionization of Liquid Polyols. II. Propanediols. *J. Phys. Chem. A* **2007**, *111*, 4902−4913.
(79) Bonin, J.; Lampre, I.; Pernot, P.; Mostafavi, M. Solvation Dynamics of Electron Produced by Two-Photon Ionization of Liquid Polyols. III. Glycerol. *J. Phys. Chem. A* **2008**, *112*, 1880−1886.
(80) Lund, A.; Schlick, S. Trapped Electrons in Crystalline Media. *Res. Chem. Intermed.* **1989**, *11*, 37−66.
(81) Shkrob, I. A. On the Nature of Infrared Absorbing Trapped Electron Center in Low-Temperature Ice-I_h. *Chem. Phys. Lett.* **2007**, *443*, 289−292.
(82) Wishart, J. F.; Neta, P. Spectrum and Reactivity of the Solvated Electron in the Ionic Liquid Methyltributylammonium Bis-(Trifluoromethylsulfonyl)Imide. *J. Phys. Chem. B* **2003**, *107*, 7261−7267.
(83) Wishart, J. F.; Shkrob, I. A. The Radiation Chemistry of Ionic Liquids and Its Implications for Their Use in Nuclear Fuel Processing. In *Ionic Liquids: From Knowledge to Application*; Plechkova, N. V., Rogers, R. D., Seddon, K. R., Eds.; American Chemical Society: Washington, DC, 2009; pp 119−134.
(84) Wishart, J. F. Ionic Liquids and Ionizing Radiation: Reactivity of Highly Energetic Species. *J. Phys. Chem. Lett.* **2010**, *1*, 3225−3231.
(85) Muller, E. A.; Strader, M. L.; Johns, J. E.; Yang, A.; Caplins, B. W.; Shearer, A. J.; Suich, D. E.; Harris, C. B. Femtosecond Electron Solvation at the Ionic Liquid/Metal Electrode Interface. *J. Am. Chem. Soc.* **2013**, *135*, 10646−10653.
(86) Molins i Domenech, F.; FitzPatrick, B.; Healy, A. T.; Blank, D. A. Photodetachment and Electron Reactivity in 1-Methyl-1-Butyl-Pyrrolidinium Bis(Trifluoromethylsulfonyl)Amide. *J. Chem. Phys.* **2013**, *137*, 034512.
(87) Saenko, E. V.; Takahashi, K.; Feldman, V. I. EPR Evidence for a Physically Trapped Excess Electron in a Glassy Ionic Liquid. *J. Phys. Chem. Lett.* **2013**, *4*, 2896−2899.
(88) Shkrob, I. A. The Structure and Dynamics of Solvated Electrons. In *Recent Trends in Radiation Chemistry*; Wishart, J. F., Rao, B. S. M., Eds.; World Scientific Publishing: Singapore, 2010; pp 59−97.
(89) Shkrob, I. A.; Sauer, M. C. Photostimulated Electron Detrapping and the Two-State Model for Electron Transport in Nonpolar Liquids. *J. Chem. Phys.* **2005**, *122*, 134.
(90) Silva, C.; Walhout, P. K.; Reid, P. J.; Barbara, P. F. Detailed Investigations of the Pump−Probe Spectroscopy of the Equilibrated Solvated Electron in Alcohols. *J. Phys. Chem. A* **1998**, *102*, 5701−5707.
(91) Tabata, Y.; Ito, Y.; Tagawa, S. *CRC Handbook of Radiation Chemistry*; CRC Press, Inc.: Boca Raton, 2000; pp 395−438.
(92) Samskog, P.-O.; Lund, A.; Nilsson, G.; Symons, M. C. R. Primary Reactions of Localized Electrons in Rhamnose Crystals Studied by Pulse Radiolysis and ESR Spectroscopy. *J. Chem. Phys.* **1980**, *73*, 4862−4866.
(93) Samskog, P.-O.; Lund, A.; Nilsson, G. Localized Electrons in 1,8-Octanediol Crystals Studied by ESR Spectroscopy and Pulse Radiolysis. *Chem. Phys. Lett.* **1981**, *79*, 447−451.
(94) Lindgren, M.; Lund, A.; Ogasawara, M.; Samskog, P.-O. Localized Electron to Radical Conversion in X-Irradiated Single Crystals of 1,6-Hexanediol and 1,8-Octanediol. *Radiat. Phys. Chem.* **1987**, *29*, 439−445.
(95) Poupko, R.; Loewenstein, A. Kinetic Study of Proton Exchange in Radicals Derived from Simple Alcohols. *J. Chem. Soc. A* **1968**, 949−951.
(96) Koksal, F.; Celik, F. Electron Spin Resonance of a Gamma-Irradiated Single Crystal of Carbamylcholine Chloride. *J. Chem. Soc., Faraday Trans. I* **1988**, *84*, 2305−2309.
(97) Yoshizawa-Fujita, M.; Kousa, Y.; Kidena, K.; Ohira, A.; Takeoka, Y.; Rikukawa, M. Proton Transport Properties in an Ionic Liquid Having a Hydroxyl Group. *Phys. Chem. Chem. Phys.* **2011**, *13*, 13427−13432.
(98) Becke, A. D. Density-Functional Exchange-Energy Approximation with Correct Asymptotic Behavior. *Phys. Rev. A* **1988**, *38*, 3098−3100.
(99) Lee, C.; Yang, W.; Parr, R. G. Development of the Colle-Salvetti Correlation-Energy Formula into a Functional of the Electron Density. *Phys. Rev. B* **1988**, *37*, 785−789.
(100) Frisch, M. J.; Trucks, G. W.; Schlegel, H. B.; Scuseria, G. E.; Robb, M. A.; Cheeseman, V. G.; Montgomery, J. A., Jr.; Vreven, K. N.; Kudin, J. C.; Burant, J. C. *Gaussian 03*, revision C.02; Gaussian, Inc., Wallingford, CT, 2004.
(101) Wishart, J. F.; Cook, A. R.; Miller, J. R. The Leaf Picosecond Pulse Radiolysis Facility at Brookhaven National Laboratory. *Rev. Sci. Instrum.* **2004**, *75*, 4359−4366.
(102) Wishart, J. F.; Funston, A. M.; Szreder, T.; Cook, A. R.; Gohdo, M. Electron Solvation Dynamics and Reactivity in Ionic Liquids Observed by Picosecond Radiolysis Techniques. *Faraday Discuss.* **2012**, *154*, 353−363.
(103) Grills, D. C.; Cook, A. R.; Fujita, E.; George, M. W.; Preses, J. M.; Wishart, J. F. Application of External-Cavity Quantum Cascade Infrared Lasers to Nanosecond Time-Resolved Infrared Spectroscopy of Condensed-Phase Samples Following Pulse Radiolysis. *Appl. Spectrosc.* **2010**, *64*, 563−570.
(104) Grills, D. C.; Farrington, J.; Layne, B. H.; Lymar, S. V.; Mello, B. A.; Preses, J. M.; Wishart, J. F. Mechanism of the Formation of a Mn-Based CO_2 Reduction Catalyst Revealed by Pulse Radiolysis with Time-Resolved Infrared Detection. *J. Am. Chem. Soc.* **2014**, *136*, 5563−5566.
(105) Shkrob, I. A.; Chemerisov, S. D. Light Induced Fragmentation of Polyfunctional Carboxylated Compounds on Hydrated Metal Oxide Particles: From Simple Organic Acids to Peptides. *J. Phys. Chem. C* **2009**, *113*, 17138−17150.
(106) Shkrob, I. A.; Chemerisov, S. D.; Marin, T. W. Photocatalytic Decomposition of Carboxylated Molecules on Light-Exposed Martian Regolith and Its Relation to Methane Production on Mars. *Astrobiology* **2010**, *10*, 425−436.
(107) Shkrob, I. A.; Marin, T. W.; Chemerisov, S. D.; Hatcher, J. L.; Wishart, J. F. Toward Radiation-Resistant Ionic Liquids. Radiation

Stability of Sulfonyl Imide Anions. *J. Phys. Chem. B* **2012**, *116*, 9043−9055.
(108) Shkrob, I. A.; Marin, T. W.; Wishart, J. F. Ionic Liquids Based on Polynitrile Anions: Hydrophobicity, Low Proton Affinity, and High Radiolytic Resistance Combined. *J. Phys. Chem. B* **2013**, *117*, 7084−7094.
(109) Shkrob, I. A.; Wishart, J. F. Charge Trapping in Imidazolium Ionic Liquids. *J. Phys. Chem. B* **2009**, *113*, 5582−5592.
(110) Funston, A. M.; Wishart, J. F. Dynamics of Fast Reactions in Ionic Liquids. In *Ionic Liquids IIIA: Fundamentals, Progress, Challenges, and Opportunities, Properties and Structure*; Rogers, R. D., Seddon, K. R., Eds.; American Chemical Society: Washington, DC, 2005; Vol. *901*, pp 102−116.
(111) Wishart, J. F.; Lall-Ramnarine, S. I.; Raju, R.; Scumpia, A.; Bellevue, S.; Ragbir, R.; Engel, R. Effects of Functional Group Substitution on Electron Spectra and Solvation Dynamics in a Family of Ionic Liquids. *Radiat. Phys. Chem.* **2005**, *72*, 99−104.
(112) Musat, R. M.; Kondoh, T.; Yoshida, Y.; Takahashi, K. Twin-Peaks Absorption Spectra of Excess Electron in Ionic Liquids. *Radiat. Phys. Chem.* **2014**, *100*, 32−37.
(113) Nielsen, S. O.; Michael, B. D.; Hart, E. J. Ultraviolet-Absorption Spectra of e_{aq}^-, H, OH, D and OD from Pulse Radiolysis of Aqueous-Solutions. *J. Phys. Chem.* **1976**, *80*, 2482−2488.
(114) Belloni, J.; Billiau, F.; Saito, E. Ultraviolet-Absorption of the Solvated Electron in Ammonia and Deuteroammonia Solutions. *Nouv. J. Chim.* **1979**, *3*, 157−161.
(115) Jou, F.-Y.; Freeman, G. R. Shapes of Optical Spectra of Solvated Electrons. Effect of Pressure. *J. Phys. Chem.* **1977**, *81*, 909−915.
(116) Lin, M.; Mostafavi, M.; Muroya, Y.; Han, Z.; Lampre, I.; Katsumura, Y. Time-Dependent Radiolytic Yields of the Solvated Electrons in 1,2-Ethanediol, 1,2-Propanediol, and 1,3-Propanediol from Picosecond to Microsecond. *J. Phys. Chem. A* **2006**, *110*, 11404−11410.
(117) Wishart, J. F. Ionic Liquid Radiation Chemistry. In *Ionic Liquids Further Uncoiled: Critical Expert Overviews*; Plechkova, N., Seddon, K. R., Eds.; Wiley, Ltd.: Chichester, UK, 2014; pp 259−274.
(118) Cederstav, A. K.; Novak, B. M. Investigations into the Chemistry of Thermodynamically Unstable Species. The Direct Polymerization of Vinyl Alcohol, the Enolic Tautomer of Acetaldehyde. *J. Am. Chem. Soc.* **1994**, *116*, 4073−4074.
(119) Nagaoka, M.; Suenobu, K.; Yamabe, T. On the Hydronium Ion Catalyzed Mechanism in Vinyl Alcohol−Acetaldehyde Isomerization: Ab Initio Molecular Orbital Theory and Monte Carlo Simulation. *J. Am. Chem. Soc.* **1997**, *119*, 8023−8030.
(120) Bennett, C. J.; Osamura, Y.; Lebar, M. D.; Kaiser, R. I. Laboratory Studies on the Formation of Three C_2H_4O Isomers - Acetaldehyde (CH_3CHO), Ethylene Oxide (c-C_2H_4O), and Vinyl Alcohol (CH_2CHOH) - in Interstellar and Cometary Ices. *Astrophys. J.* **2005**, *634*, 698−711.
(121) Harmon, K. M.; Gunsel, F. A. Hydrogen Bonding. Part 20. Infrared Study of the High Temperature Beta-Form of Choline Chloride. *J. Mol. Struct.* **1986**, *140*, 261−268.